7-2019

In Vivo Human-Like Robotic Phenotyping of Leaf and Stem Traits in Maize and Sorghum in Greenhouse

Abbas Atefi
University of Nebraska-Lincoln, abbas.atefi@huskers.unl.edu

IN VIVO HUMAN-LIKE ROBOTIC PHENOTYPING OF LEAF AND STEM TRAITS IN MAIZE AND SORGHUM IN GREENHOUSE

by

Abbas Atefi

A DISSERTATION

Presented to the Faculty of

The Graduate College at the University of Nebraska

In Partial Fulfilment of Requirements

For the Degree of Doctor of Philosophy

Major: Biological Engineering

Under the Supervision of Professors Yufeng Ge and Santosh Pitla

Lincoln, Nebraska

July, 2019

IN VIVO HUMAN-LIKE ROBOTIC PHENOTYPING OF LEAF AND STEM TRAITS IN MAIZE AND SORGHUM IN GREENHOUSE

Abbas Atefi, Ph.D.
University of Nebraska, 2019

Advisors: Yufeng Ge, Santosh Pitla

In plant phenotyping, the measurement of morphological, physiological and chemical traits of leaves and stems is needed to investigate and monitor the condition of plants. The manual measurement of these properties is time consuming, tedious, error prone, and laborious. The use of robots is a new approach to accomplish such endeavors, which enables automatic monitoring with minimal human intervention. In this study, two plant phenotyping robotic systems were developed to realize automated measurement of plant leaf properties and stem diameter which could reduce the tediousness of data collection compare to manual measurements. The robotic systems comprised of a four degree of freedom (DOF) robotic manipulator and a Time-of-Flight (TOF) camera. Robotic grippers were developed to integrate an optical fiber cable (coupled to a portable spectrometer) for leaf spectral reflectance measurement, a thermistor for leaf temperature measurement, and a linear potentiometer for stem diameter measurement. An Image processing technique and deep learning method were used to identify grasping points on leaves and stems, respectively. The systems were tested in a greenhouse using maize and sorghum plants. The results from the leaf phenotyping robot experiment showed that leaf temperature measurements by the phenotyping robot were correlated with those measured manually by a human researcher (R^2 = 0.58 for maize and 0.63 for sorghum).

The leaf spectral measurements by the phenotyping robot predicted leaf chlorophyll, water content and potassium with moderate success (R^2 ranged from 0.52 to 0.61), whereas the prediction for leaf nitrogen and phosphorus were poor. The total execution time to grasp and take measurements from one leaf was 35.5±4.4 s for maize and 38.5±5.7 s for sorghum. Furthermore, the test showed that the grasping success rate was 78% for maize and 48% for sorghum. The experimental results from the stem phenotyping robot demonstrated a high correlation between the manual and automated stem diameter measurements ($R^2 > 0.98$). The execution time for stem diameter measurement was 45.3 s. The system could successfully detect and localize, and also grasp the stem for all plants during the experiment. Both robots could decrease the tediousness of collecting phenotypes compare to manual measurements. The phenotyping robots can be useful to complement the traditional image-based high-throughput plant phenotyping in greenhouses by collecting in vivo morphological, physiological, and biochemical trait measurements for plant leaves and stems.

ACKNOWLEDGMENTS

I would like to express my sincere gratitude to my advisors Dr. Yufeng Ge and Dr. Santosh Pitla for the continuous support, and motivation they have provided through my Ph.D study and related research with great patience and immense knowledge. Their inspiration and guidance helped me in all the time of research and writing of this dissertation.

Besides my advisors, I would like to thank the rest of my committee members: Dr. James Schnable, and Dr. Benjamin Terry, for their insightful comments and invaluable advice.

I thank my friends Nuwan Wijewardane, Piyush Pandey, Suresh Thapa, Geng Bai, Ujjwol Bhandari, Wenan Yuan, Jasreman Singh, Alessandro Amaranto, and Chee Town Liew for their help in my research and giving me good ideas and suggestions in general. I am also thankful to greenhouse staff Vincent Stoerger, Troy Pabst, and Nathan Duffy for their assistance in conducting experiments at phenotyping greenhouse facility on UNL's Innovation Campus, and undergraduate student Ema Muslic for her assistance in data collection. I would also like to acknowledge USDA-NIFA (Award# 2017-67007-25941) to provide funding for this research.

Last but not the least, I would like to express my very profound gratitude to my parents and siblings for their warm love, endless support, and continuous encouragement throughout my years of study and process of researching, writing this dissertation, and my life in general.

TABLE OF CONTENTS

LIST OF FIGURES

LIST OF TABLES

CHAPTER 1

INTRODUCTION

1.1 PLANT BREEDING

Plant breeding is the science of changing the traits of plants in order to improve their genetic potential and produce desired characteristics. The goal of plant breeding is to improve the performance of the plant. The breeders try to improve the productivity of crops by increasing their yield and quality. Higher yield of crops helps to supply more food, increases the profit of agricultural products, and reduces the cost of food for the consumers. Improved quality may contribute to produce more nutritious food and decrease the presence of toxic compounds. The yield and quality of crops can be increased by breeding the plants for disease or insect resistance, which leads to improving the health of plants and also an environmentally practice as fewer protective chemicals will be utilized in the cultivation of the resistant plants. Plant breeders develop new varieties which are adapted to a wide range of production areas and tolerant to adverse environmental production hazards such as drought, extremes of temperature, and salinity (Poehlman, 2013).

Plant breeding methods change over time. The breeders just relied on their skill to visually judge about the appearance, or phenotype, of a plant in order to select the most desirable plants in the beginning of plant selection (Fehr, 1991). However, it is now possible for breeders to use advanced techniques in genetics such as next generation

DNA sequencing for genetic improvement which has accelerated traditional methods by molecular breeding (Fahlgren et al., 2015a).

Population increases, climate change, degradation and loss of arable land, and the increasing appearance of new pests and diseases are expected to threaten global food security over the next century (Fischer, 2009). However, the increase of average rate of crop production using the traditional breeding is no longer sufficient to meet the projected demand (Phillips, 2010). Although molecular breeding methods use genotypic information for selection process, they still need to quantify plant traits (phenotypes) (Jannink et al., 2010). On the other hand, the lack of access to plant phenotyping data causes limitation to dissect the genetics of quantitative traits which are related to growth, yield and adaptation to stress (McMullen et al., 2009).

Understanding how plants respond to environmental and genetic perturbations is essential to accelerating the improvement of crop yield for food, feed, and fuel using fewer input resources (Chaves et al., 2003). Fig.1.1 indicates the relationship between plant genotype, phenotype, and environment.

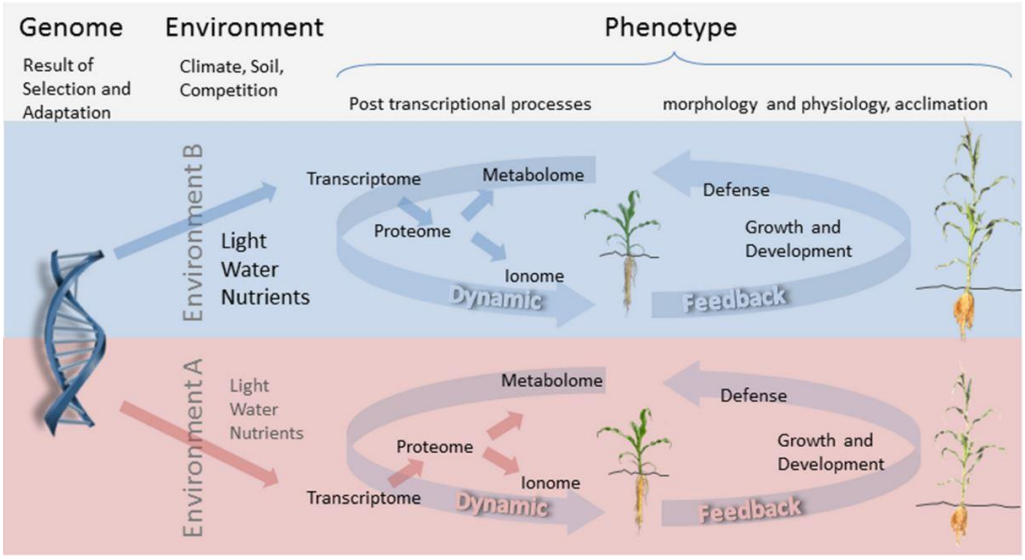

Fig. 1.1. Relationship between plant genotype, phenotype, and environment (source: Walter et al., 2015)

1.2 PLANT PHENOTYPING

Plant phenotyping is the quantitative and qualitative assessment of structural, physiological, bio-chemical, and performance-related traits of plant at any organizational level (ranging from the field and canopy, to the whole-plant, organ, tissue, and cellular level) of a given genotype in a given environment (Dhondt et al., 2013). Plant phenotype is the set of these complex traits. Parameters such as biomass, leaf characteristics, stem characteristics, photosynthetic efficiency, yield-related traits, and stress response are the direct examples of these traits (Li et al., 2014) (Fig.1.2).

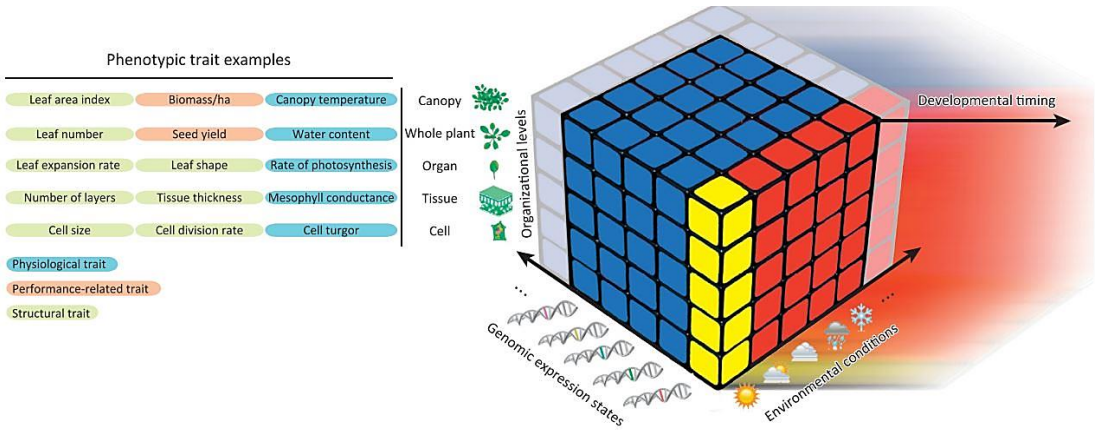

Fig. 1.2. The structural and physiological, and performance-related traits of plant (source: Dhondt et al., 2013)

Plant phenotyping studies the interaction between the environmental factors and plant phenotypes (Foix et al., 2015). This interaction between the phenotypes and the environment influences the developmental program and growth of plants (structural traits) and also plant functioning (physiological traits). Eventually the plant performance (biomass and yield) will be determined by both structural and physiological traits (Granier and Tardieu, 2009). Today, plant phenotyping became an applicable tool for plant breeders to select desirable genotypes and identify the best genetic variation (Walter et al., 2015).

It is important to extract data and perform quantitative assessment of the plant phenotypes from a series of long-term monitoring experiments over a large number of plants under multiple environmental conditions (Foix et al., 2018). Currently, the destructive sampling methods at fixed times or at particular phenological stages have been used to collect and investigate plant phenotypes (Furbank and Tester, 2011). The destructive methods do not permit temporal examination of traits in individual plants,

accordingly the number of plants needed to be examined will be increased (Fahlgren et al., 2015a). Moreover, because this method is labor-intensive and costly, many plant breeders solely make a single measurement of final yield of crop for replicated plots (Furbank and Tester, 2011). Yield itself is one of the most poorly inherited traits in crop breeding (Richards et al., 2010).

Conventional plant phenotyping relies largely on visual scoring by experts, which is labor-intensive, costly, time-consuming and prone to error (Vijayarangan et al., 2018). Plant breeders want to increase breeding efficiency by collecting the phenotypic data of large numbers of lines rapidly and accurately (McMullen et al., 2009). The plant traits can be examined temporally using non-invasive and non-destructive techniques which reduce the number of plants needed and allow the examination of larger populations. In recent years, automated workflows have been used to process and monitor several hundreds of plants daily with minimal human intervention by combining novel technologies such as non-invasive and non-destructive image-based phenotyping techniques, machine learning (deep learning), spectroscopy, image analysis, and robotics to address the aforementioned phenotyping bottleneck (Furbank and Tester, 2011).

1.3 AUTOMATED PHENOTYPING PLATFORMS

The scale of phenotyping platforms is varied from proximal to remote sensing. These platforms allow to monitor single leaves/plant organs, individual plants, field plots and full fields precisely and consistently (Fig. 1.3). Different types of architectures including unmanned aerial vehicles (UAV)/drones, autonomous ground vehicles/rovers, phenotyping towers, field scanning platforms, image-based phenotyping platforms, and robotic manipulators are used as automated phenotyping platforms (Shakoor et al., 2017).

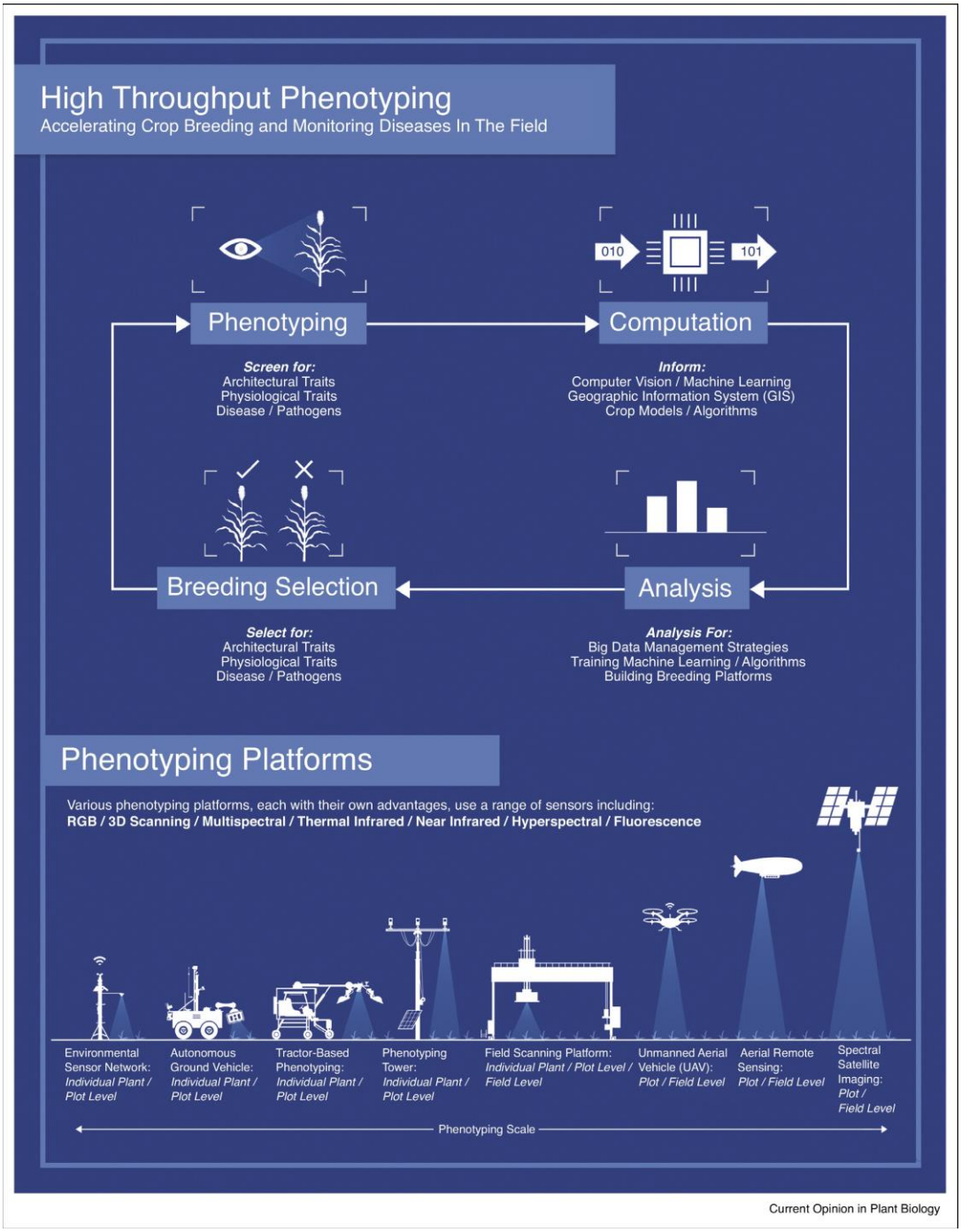

Fig. 1.3. Scales of automated phenotyping platforms (source: Shakoor et al., 2017)

Unmanned Aerial Vehicle (UAV): UAV (drone) refers to a type of aircraft which operates with no pilot on board. A wide range of sensors such as fluorescence sensors, digital cameras (red-green-blue (RGB)), multispectral or color-infrared cameras, and thermal sensors can be integrated to UAVs to collect aerial imagery with very high spatial and temporal resolutions (Holman et al., 2016). Agricultural drones are used as data acquisition systems for field phenotyping. They capture plant characteristics by acquiring images over large landscape which can be used to evaluate plant performance (yield prediction) and detect plant stress and diseases during breeding (Chapman et al., 2014).

Zaman-Allah et al. (2015) proposed the use of UAV equipped with a multi-spectral sensor for field phenotyping of maize. The aerial platform was used to investigate the low-nitrogen stress tolerance in maize. Overall, the results showed that the Normalized Difference Vegetation Index (NDVI) data which were derived from the aerial imagery had a high correlation with ground-truth NDVI and grain yield. Furthermore, the aerial sensing platform has an effective contribution to assess the crop performance under the stress. Holman et al. (2016) utilized a UAV with RGB camera to derive the height and growth rate of wheat plants. The aerial imagery collected by the UAV was used to reconstruct 3D digital surface models of crop field via Structure from Motion (SfM) photogrammetry. The comparison between UAV derived and manual measurement of crop heights showed that the two sets of measurements were highly correlated with $R^2 \geq 0.92$ and Root Mean Squared Error (RMSE) ≤ 0.07 m. The results proved that UAV based SfM had the potential to monitor plant height throughout the season and collected rapid and accurate measurement of crop height as well as growth rate calculation.

Berni et al. (2009) used a helicopter-based UAV with thermal and narrowband multi-spectral imaging sensors to obtain surface reflectance and temperature for vegetation monitoring purpose. Several vegetation indices such as NDVI, transformed chlorophyll absorption in reflectance index/optimized soil-adjusted vegetation index, and photochemical reflectance index (PRI) were calculated based on the data of the multi-spectral sensors for a corn field. The validation results showed successful estimation for Leaf Area Index (LAI), and chlorophyll concentration of canopy. It also demonstrated a high correlation between the PRI and canopy temperature which is a good indicator for water stress detection. Yue et al. (2017) estimated above-ground biomass (AGB) of winter wheat using the images of a hyperspectral sensor which was mounted on a UAV. The crop height and canopy reflectance were obtained from the data of a hyperspectral sensor. They constructed a model based on crop height combined with specific bands and vegetation indices to predict crop AGB. Comparison with experimental results indicated that their method had promising accuracy for winter wheat AGB estimation. Li et al. (2018) used a UAV equipped with a true-color RGB camera and a 5-band multi-spectral camera to elucidate biomass, nitrogen and chlorophyll content of sorghum under nitrogen stress treatments. Morphological and spectral traits including plant height, canopy cover and various vegetation indices were derived from the data which were collected at different growth stages during the growing season. The result showed that UAV-derived canopy height, biomass, nitrogen content, and chlorophyll content were strongly correlated with the manual measurements.

Image-based phenotyping: Image-based approach in plant phenotyping is a growing application area of computer vision in agriculture to measure plant morphological and chemical traits rapidly and nondestructively. This approach is used to accelerate high-throughput plant phenotyping that would eventually enable effective use of genomic data to bridge the genotype-to-phenotype gap for crop improvement (Furbank and Tester, 2011; Fahlgren et al., 2015b) (Fig. 1.4).

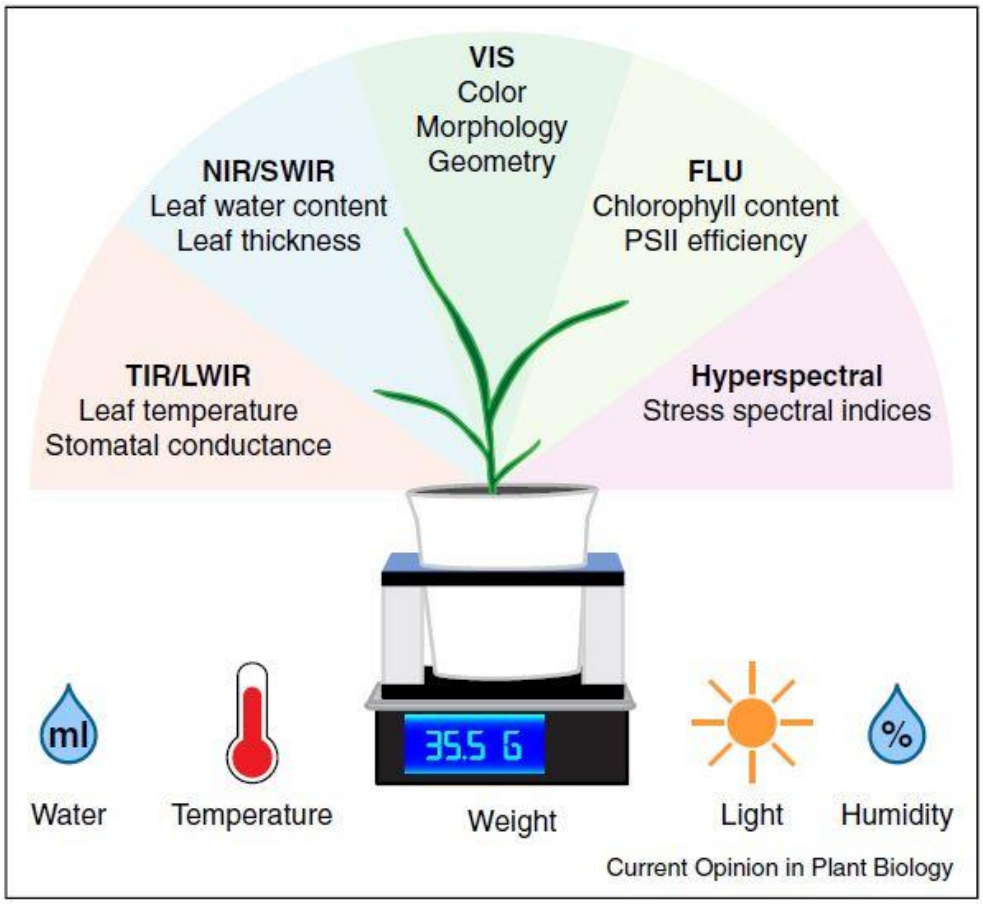

Fig. 1.4. High-throughput phenotyping platform collect images, environmental and physical data to measure plant phenotypes (source: Fahlgren et al., 2015b)

Hairmansis et al. (2014) developed a non-destructive image-based phenotyping protocol to investigate the response of two rice cultivars to different levels of salt stress.

Visible (RGB) and fluorescence images were used to quantify total shoot area and senescent shoot area. The reduced increase of shoot area was a good indicator to distinguish the stressed plants from the control and it made the technique as a useful tool to assess salinity tolerance traits in rice. Pandey et al. (2017) established a high-throughput method which could quantify the chemical properties of maize and soybean plants. For this purpose, they utilized hyperspectral images of the plants to estimate leaf water content, as well as concentrations of macronutrients such as nitrogen (N), phosphorus (P), potassium (K) and micronutrients such as sodium (Na), iron (Fe), manganese (Mn). A model based on Partial Least Square Regression (PLSR) was developed to correlate the spectral data with the chemical properties of leaf. They reported that water content was predicted with the highest accuracy and macronutrients were quantified satisfactorily such that their prediction accuracy was higher than the micronutrients. Gage et al. (2017) presented a tassel image-based phenotyping system (TIPS) which provided a platform to quantify the morphological features of maize tassels automatically. They used digital camera to acquire the images form freshly harvested tassels for different lines of maize in field. The correlation between manual measurements of tassel traits (tassel weight, tassel length, spike length, and branch number) with automated measurements ranged from 0.66 to 0.89. The image-based phenotyping system also could quantify additional tassel characteristics (curvature, compactness, fractal dimension, skeleton length, and perimeter) which can not be measured manually. Thapa et al. (2018) developed a LiDAR (light detection and ranging)-based phenotyping for 3D measurement of morphological traits in maize and sorghum. Plant leaf surface was reconstructed using 3D point clouds of plant, and plant

morphological traits including individual and total leaf area, leaf inclination angle, and leaf angular distribution were derived. The results showed a high correlation between LiDAR-based and reference methods for leaf area measurements. Choudhury et al. (2016) used visible light images (from publicly available Panicoid Phenomap-1 dataset) to facilitate vegetative stage phenotyping analysis of maize. They developed two automated software packages to compute two new holistic phenotypes, namely, bi-angular convex-hull area ratio and plant aspect ratio which explain phyllotaxy and canopy architecture of different genotypes of maize plants respectively. An algorithm also was introduced to compute component-based phenotypes, i.e., total number of leaves and size of each leaf of a plant.

Since the image processing pipelines have limited flexibility and poor performance for complex phenotyping tasks, machine learning techniques are expected to take a prominent role in the future of image-based phenotyping (Tsaftaris et al., 2016). Deep learning is an emerging area of machine learning which is applied for large data analytics problems (Ubbens and Stavness, 2017). Convolutional neural network (CNN) is a class of deep learning methods which is most commonly used for image-based plant phenotyping tasks (Pound et al., 2017). CNN typically uses raw images directly and actively learn a variety of filter parameters during training of a model (Fig. 1.5). CNN and its variants significantly outperforms for different tasks such as regression, image classification, and object detection and segmentation (Ubbens and Stavness, 2017).

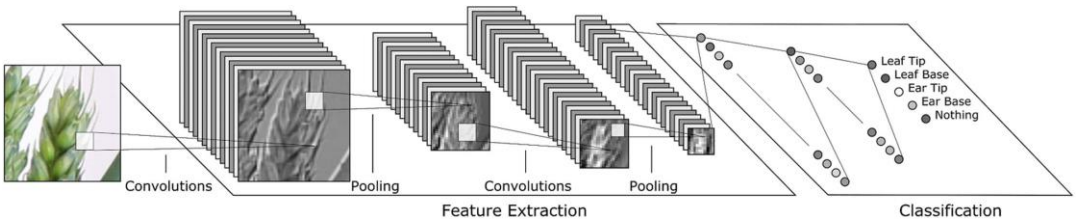

Fig. 1.5. A CNN architecture which operates on image of part of an ear of wheat (source: Pound et al., 2017)

Zhang et al. (2018) proposed two methods using improved GoogLeNet and Cifar10 models based on deep learning for leaf disease identification. The images of eight kinds of maize leaf diseases were used to train and test the modified models. Both models showed high average accuracy (> 98%) for leaf disease recognition. Ghosal et al. (2018) built a deep learning model to identify and classify a large set of foliar stresses in soybean using RGB images of soybean leaves. The deep learning framework could identify and classify several biotic (bacterial and fungal diseases) and abiotic (chemical injury and nutrient deficiency) stresses rapidly with remarkable accuracy. Pound et al. (2017) demonstrated the use of deep learning approach to identify and localize root and shoot features of wheat plant. The technique was used to localize root tip, leaf tip, leaf base, ear tip, and ear base of plant. Deep learning–based phenotyping method showed high detection and localization accuracy in validation and testing image sets.

Ground-based phenotyping: Since phenotypic responses of interest for crop improvement, especially those related to yield potential and abiotic stress tolerance, involve suites of traits that are best measured as expressed among communities of plants that grow under real world conditions which is agronomically relevant edaphic and climatic conditions, accordingly field-based systems are more readily incorporated into

applied plant breeding programs. Thus, there is growing interest in adapting agricultural machinery and electronic sensors to build systems that can collect multi-modal, multi-character data for phenotyping plants real-time in the field (Montes et al., 2007; White et al., 2012). Consequently, various vehicle-based systems were used or proposed for field-based high-throughput plant phenotyping. Andrade-Sanchez et al. (2013) developed a high-throughput phenotyping platform to measure the dynamic traits of cotton in the field. Four sets of sensors were carried by the system to measure canopy height, NDVI, and temperature simultaneously on four adjacent rows. The high-throughput measurements of canopy height, NDVI, and temperature indicated a strong agreement with the manual measurements of the plant phenotypes. The results confirmed that multiple traits can be measured by the system rapidly and accurately. Busemeyer et al. (2013) established a tractor-pulled multi-sensor platform for non-destructive field-based phenotyping. Several sensors such as light curtain imaging, 3D TOF cameras, laser distance sensors, hyperspectral imaging, and color imaging were integrated into the system to collect spectral and morphological information of small grain cereals. High technical repeatability of measurement results from all different sensors illustrated high suitability and robustness of the developed platform for field-phenotyping in plant breeding trials. Barker et al. (2016) developed a field-based high-throughput mobile phenotyping platform to measure the characteristics of wheat and soybean. Three sets of sensors were mounted on a high-clearance vehicle, thus three plots were measured simultaneously in a single pass. Each set of sensors compromised of two infrared thermometers (IRT), one ultrasonic sensor, one Crop Circle multi-spectral crop canopy sensor, and one GreenSeeker crop sensing system to measure canopy temperature, crop

height, and canopy spectral reflectance of a plant plot. The system verification test indicted great potential of the platform for broad application to address a range of questions regarding crop canopy characteristics. Bai et al., (2016) reported a high-throughput multi-sensor system to phenotype soybean and wheat plants. Five sensor modules (ultrasonic distance sensors, thermal infrared radiometers, NDVI sensors, portable spectrometers, and RGB web cameras) were used to measure crop canopy traits from field plots. The experimental results showed that the system had satisfactorily and robust performance to collect field-based, high-throughput plant phenotyping data. Yuan et al. (2018) proposed a ground-based multi-sensor phenotyping system which equipped with ultrasonic sensors and LiDAR to estimate canopy heights of wheat plots. The experimental results demonstrated that the proposed LiDAR-based method could provide precise and accurate plant height estimates. Bao et al. (2019) presented a high-throughput field-based robotic phenotyping system which included multilevel side-viewing stereo camera heads installed on an auto-steer tractor to measure architectural traits of sorghum plants. They developed an automated feature extraction pipeline which could quantify plot-based plant height, plot-based plant width, convex hull volume, plant surface area, and stem diameter (semiautomated). The experimental results showed a high correlation between the image-derived measurements and in-field manual measurements. Shafiekhani et al. (2017) introduced two robotic platforms for high-throughput field-phenotyping. The robotic architecture consisted of two robotic platforms: an autonomous ground vehicle (Vinobot) and a mobile observation tower (Vinoculer) which could collect data from individual plants and oversee an entire field, identifying specific plants for further inspection respectively. The comparison results between the phenotypes which

was taken by the robotic platforms and phenotype data which was collected by hand demonstrated that the proposed architecture was reliable, versatile, and extendable.

Robotic manipulator/arm: Robotic manipulators perform best when they are used in structured environments where their desired tasks are known before their execution. However, the field of robotics is expanding into broader applications and the demand of using robotic manipulators to accomplish unstructured tasks which have elements that can not be known ahead of time (such as acquiring plant phenotypes) is increasing. Alenyà et al. (2011) developed a method for modeling and monitoring plant leaves using fused depth/color images. They mounted TOF and color cameras, and a probing tool on the end-effector of a robotic manipulator. Quadratic surface fitting was applied to segment plant images using TOF depth data. The results showed that the obtained surface fit well with the target leaves and the candidate leaves could be reached by the probing tool.

1.4 GOAL AND OBJECTIVES OF THE STUDY

The goal of this study was to develop a robotic system for *in vivo*, human-like phenotyping of maize and sorghum plants in the greenhouse which could reduce the tediousness of phenotypes measurements compare to manual measurements. There were two objectives to achieve this goal. The first objective was to develop an automated robotic system which could measure leaf traits such as leaf VisNIR (visible and near infrared) and leaf temperature simultaneously; and the second objective was to build a robotic system which could measure the stem diameter of plants automatically.

CHAPTER 2

IN VIVO HUMAN-LIKE ROBOTIC PHENOTYPING FOR LEAF TRAITS IN MAIZE AND SORGHUM IN GREENHOUSE

2.1 INTRODUCTION

With the increasing world population, agricultural production must increase to meet the demands of food, feed and fuel in the future (Rahaman et al., 2015). Climate change and lack of sufficient land to grow crops are the two major challenges that need to be addressed to produce more food (Fischer, 2009). To ensure global food security, it is necessary to monitor the interactions between plant genotype, phenotype, and environment to breed high-yielding and stress-tolerant plants (Shah et al., 2016). Plant phenotyping studies the interaction between the complex plant traits and the environment (Foix et al., 2015). It is important to perform quantitative assessment of the plant phenotypes during growing seasons (Dengyu et al., 2016), which entails regular sampling and measurement of hundreds or even thousands of plants (Van Henten et al., 2006; Fourcaud et al., 2008). Traditional plant phenotyping, where data collection is largely manually, is therefore laborious and prone to error (Vijayarangan et al., 2018).

Automated monitor and measurement with agricultural robotics represents a new approach to collect plant phenotypic data (Alenyà Ribas et al., 2012). In the fields, modular phenotyping systems with various degree of automation (from manually operated carts to fully automated field robots) are developed to collect a number of diverse crop traits during growing seasons (Andrade-Sanchez et al., 2014; Bai et al., 2016; Shafiekhani et al., 2017). More recently, gantry and cable-suspended integrated

sensing and robotic systems for large-scale plant phenotype data collection were developed (Virlet et al. 2017; Kirchgessner et al., 2017; Bai et al., 2019).

Robotic systems are also developed in controlled environments (e.g., greenhouse) to realize automated phenotyping at the single plant level. These systems often characterize a vision system and a robotic manipulator/gripper for automated plant and leaf detection, localization, and measurement. Chaudhury et al. (2017) attached a laser scanner to a robotic manipulator to reconstruct the 3D model of the plant and to compute its surface area and volume. A collision free robotic system was developed to probe plant leaves for indoor phenotyping (Bao et al., 2017). The system could probe all leaves of artificial plants and the average time for motion planning was 0.4 s. Ahlin et al. (2016) used an eye-in-hand camera with a six DOF robotic manipulator to grasp the leaves of artificial plants. The system used deep learning and visual-servoing to identify and grasp the leaves successfully.

Alenyà Ribas et al. (2012) attached a PMD CamBoard TOF camera to a robotic manipulator for probing the leaves of *Epipremnum Aureum* and *Anthurium Andreanum* plants. They also integrated a SPAD chlorophyll meter to the end effector of the robotic manipulator to measure the chlorophyll content of the leaves. The authors reported a success rate of 82% for leaf probing. Inaccurate estimation of the probing point due to poor model fitting or segmentation errors of the leaves was the main reason for the failure of the robotic system.

In this research, a robotic system was reported for *in vivo*, human-like phenotyping of leaf traits in maize and sorghum plants in the greenhouse which could collect data less tediously than manual measurements. Two sensing modules were integrated into the

robotic gripper: (1) an optical fiber cable to measure leaf VisNIR (visible and near infrared) reflectance spectra; and (2) a thermistor to measure leaf temperature. Leaf VisNIR spectra can further be used to infer an array of leaf chemical properties such as chlorophyll, water content and nitrogen contents (REF). To the best of knowledge, such a robotic system was not previously reported. Finally, an experiment was conducted to evaluate the performance of this robotic system.

2.2 MATERIALS AND METHODS

2.2.1 HARDWARE OF THE ROBOTIC SYSTEM

Vision system: A TOF camera (Model: SR4500, Mesa Imaging Inc., Zürich, Switzerland) was used as the vision system for the robot (Fig. 2.1). This camera has a pixel array of 176×144 and a field of view of 69°×55°. The accuracy of this camera is ±2 cm in the measurement range of 0.5-5 m. The camera provides XYZ coordinates (e.g., three channels) of each pixel of the scene in camera's coordinate system. Each channel can be used to create a grayscale image of the scene. The TOF camera was chosen because the 3D coordinates of grasping points on leaves can be directly extracted from the XYZ data of the camera.

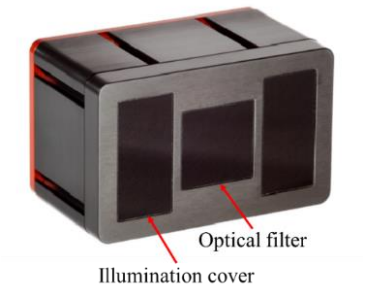

Fig. 2.1.SR4500 TOF camera and its components (source: MESA Imaging, 2016)

In Time of Flight systems, the distance between the sensor and an object is directly determined by measuring the time taken for light to travel from an active illumination source to the object and back to the sensor, given the speed of light. To achieve the time of fight measurement, the phase shift between the emmited light from the camera and the reflected light from the object is measured by a sensor of the camera. Fig. 2.2 illustrates the principle of the TOF cmera. An IR wave with 850 nm wavelength (which is indicted in red) is emmitted from an active illumination source (TOF camera) to the target object, and the reflected IR component (which is shown in blue) is detected by the sensor. The distance between the camera's coordinate system and the object is calculated using the speed of light ***c***, modulation frequency ***f***, and by measuring the phase difference between the radiated and reflected IR waves (***Δφ***).

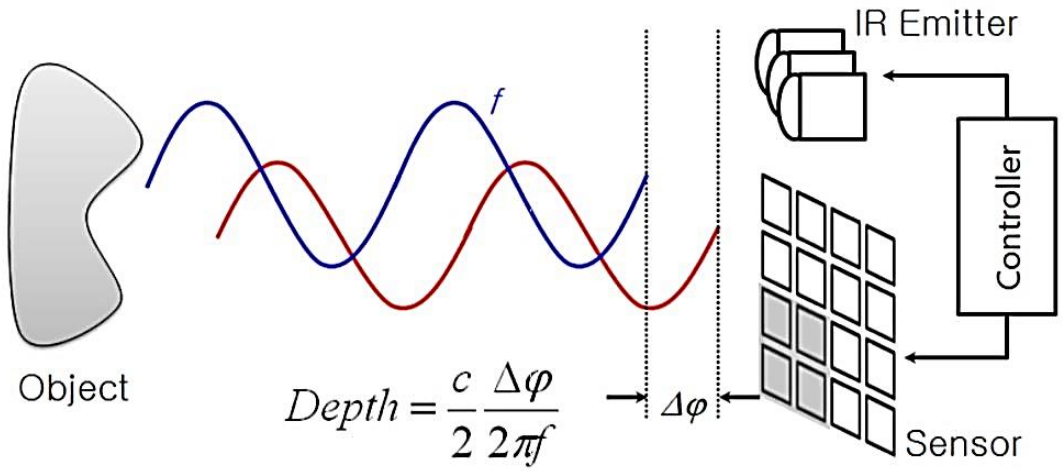

Fig. 2.2. The principle of TOF camera (source: Hansard et al., 2012)

Robotic manipulator: A four DOF robotic manipulator (Model: MICO2, KINOVA Inc., Boisbriand, Quebec, Canada) was used for this system (Fig. 2.3).

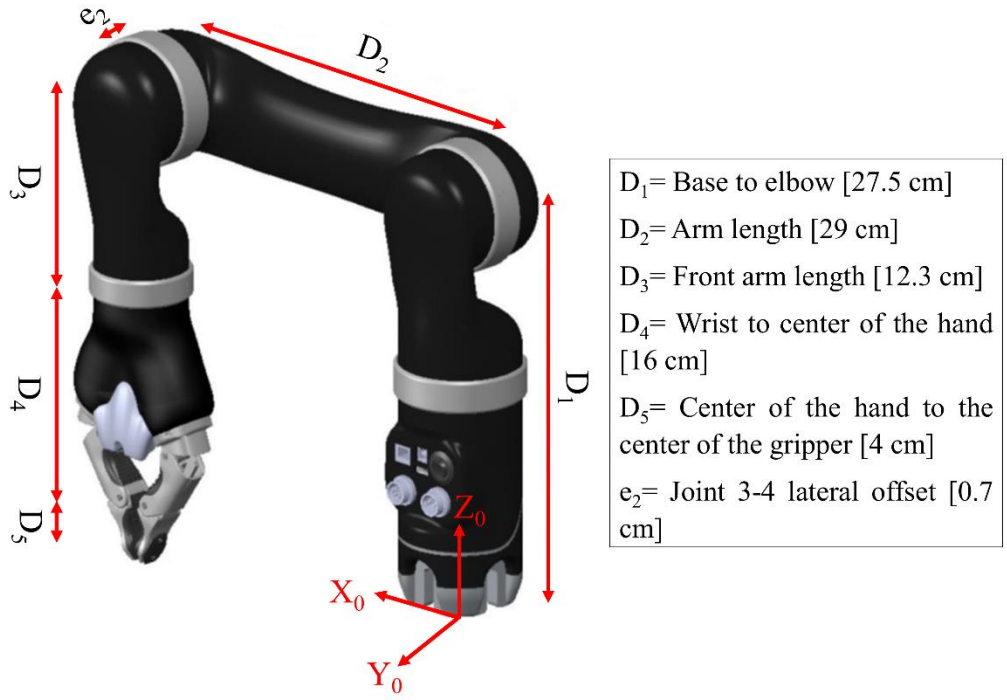

Fig. 2.3. The four degree of freedom robotic manipulator used in this study and its kinematic parameters (source: KINOVA, 2018)

The Denavit–Hartenberg (DH) parameters frame position for all joints of the robotic manipulator is shown in Fig. 2.4. Table 2.1 shows the DH parameters of the robotic manipulator.

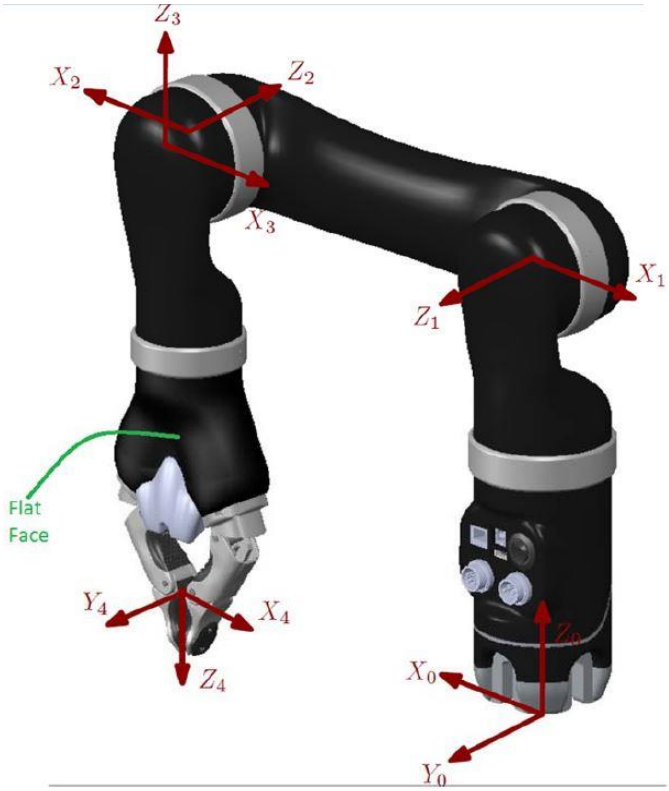

Fig. 2.4. DH parameters frame position for all joints of the robotic manipulator (source: KINOVA, 2018)

Table 2.1. DH parameters of the robotic manipulator (source: KINOVA, 2018)

i	α_{i-1}	a_{i-1}	d_i	θ_1
1	π/2	0	D_1	q_1
2	π	D_2	0	q_2
3	π/2	0	$-e_2$	q_3
4	π	0	D_3+D_4	q_4

SOLIDWORK (version 2016, DASSUALT SYSTEMS) was used to design a robotic gripper (Fig. 2.5).

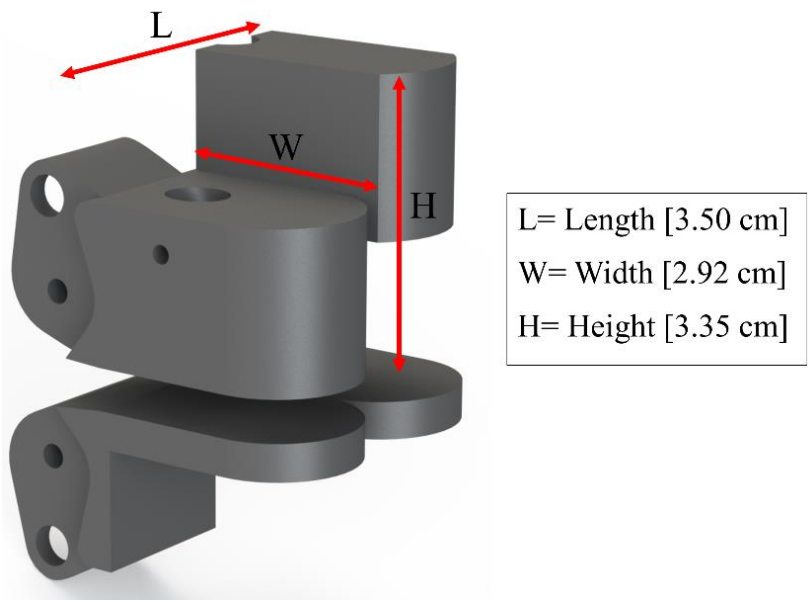

Fig. 2.5. 3D-sketch of the gripper and its dimension

The gripper was printed using a 3D printer to integrate a bifurcated optical fiber cable (for leaf VisNIR reflectance measurement) and a thermistor (for leaf temperature measurement). The gripper was printed from black plastic material to reduce the weight and minimize light scattering (Fig. 2.6). The bifurcated optical fiber cable was attached to the gripper using an adjusting set screw. A small piece of neoprene rubber with low heat conductivity was attached to the gripper in order to reduce heat transfer for leaf temperature measurement. The gripper was then attached to the end effector of the KINOVA robotic manipulator.

Fig. 2.6. The gripper and its integration to the robotic manipulator

Sensors: Fig. 2.7 shows all sensors which were used for the robotic system. The optical assembly that enabled measurement of leaf VisNIR reflectance via the bifurcated optical fiber cable (RP25, Thorlabs Inc., Newton, NJ, USA) consisted of (1) a stabilized tungsten-halogen light source (Model: SLS201, THORLABS Inc., Newton, NJ, USA) and (2) a portable spectrometer (Model: Flame, OceanOptics Inc., Dunedin, FL, USA). The output of the light source had a spectral range from 300 to 2600 nm, and the spectral range of the portable spectrometer was 350 to 1000 nm. The thermistor for leaf temperature measurement (Model: ST 200: Fine-Wire Thermistor, Apogee Instruments Inc., Logan, UT, USA) had a measurement accuracy of 0.2 °C between 0 to 70 °C and a response time of less than 1 s. The thermistor resistance is calculated using Eq. 2.1.

$$R_T = 24900\left(\frac{V_{EX}}{V_{OUT}} - 1\right) \quad (2.1)$$

Where:

R_T is the thermistor resistance in Ω which is measured by a half-bridge measurement, 24900 is the resistance of the bridge resistor in Ω, V_{EX} is the excitation input voltage (2.5 V), V_{OUT} is the output voltage of the senor in V.

From the thermistor resistance, the object temperature (T_K) in K is calculated using Steinhart-Hart equation and thermistor specific coefficients (Eq. 2.2).

$$T_K = \frac{1}{A+Bln(R_T)+C(\ln(R_T))^3} \quad (2.2)$$

Where:

$A = 1.129241 \times 10^{-3}$, $B = 2.341077 \times 10^{-4}$, and $C = 8.775468 \times 10^{-8}$ (Steinhart-Hart coefficients).

The object temperature in K (T_K) can be converted to the temperature in °C (T_C) using Eq. 2.3.

$$T_C = T_K - 273.15 \quad (2.3)$$

Fig. 2.7. (a) Light source (source: THORLABS, 2016), (b) Bifurcated optical fiber cable (source: THORLABS, 2014), (c) Portable spectrometer (source: OceanOptics, 2015), (d) Thermistor (Apogee Instruments, 2019)

A data logger (Model: LabJack U6, LabJack Corporation, Lakewood, CO, USA) was used to record data from the temperature sensor (Fig. 2.8). Three terminals of the data logger were used as an analog input which reads the output voltage from the thermistor, a terminal for excitation input voltage, and also another terminal for ground. A laptop with Intel Core i7 Processor (2.5 GHz) and 8 GB RAM was used to control the robotic system, measure and save data.

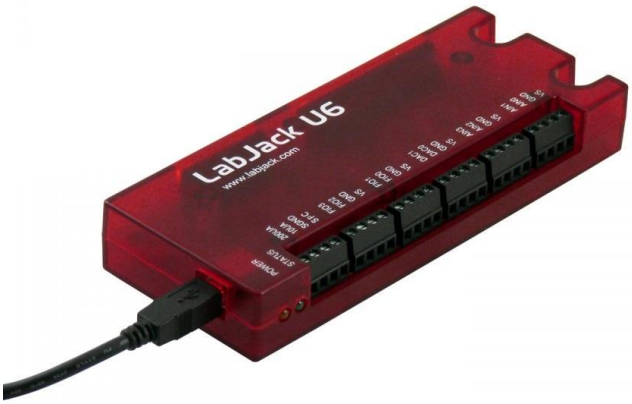

Fig. 2.8. LabJack U6 data logger (source: LabJack, 2016)

Integration of hardware for the phenotyping robotic system: The robotic system was mounted on the top of a height adjustable desk. This enabled the robotic system to adjust

its height relative to the height of plants. The camera was placed near to the robotic manipulator. The bifurcated optical fiber and the temperature sensor were integrated with the robotic manipulator by attaching them to the gripper (Fig. 2.9). Other system components including the portable spectrometer, the light source, and the data logger were also placed on the desk (Fig. 2.9).

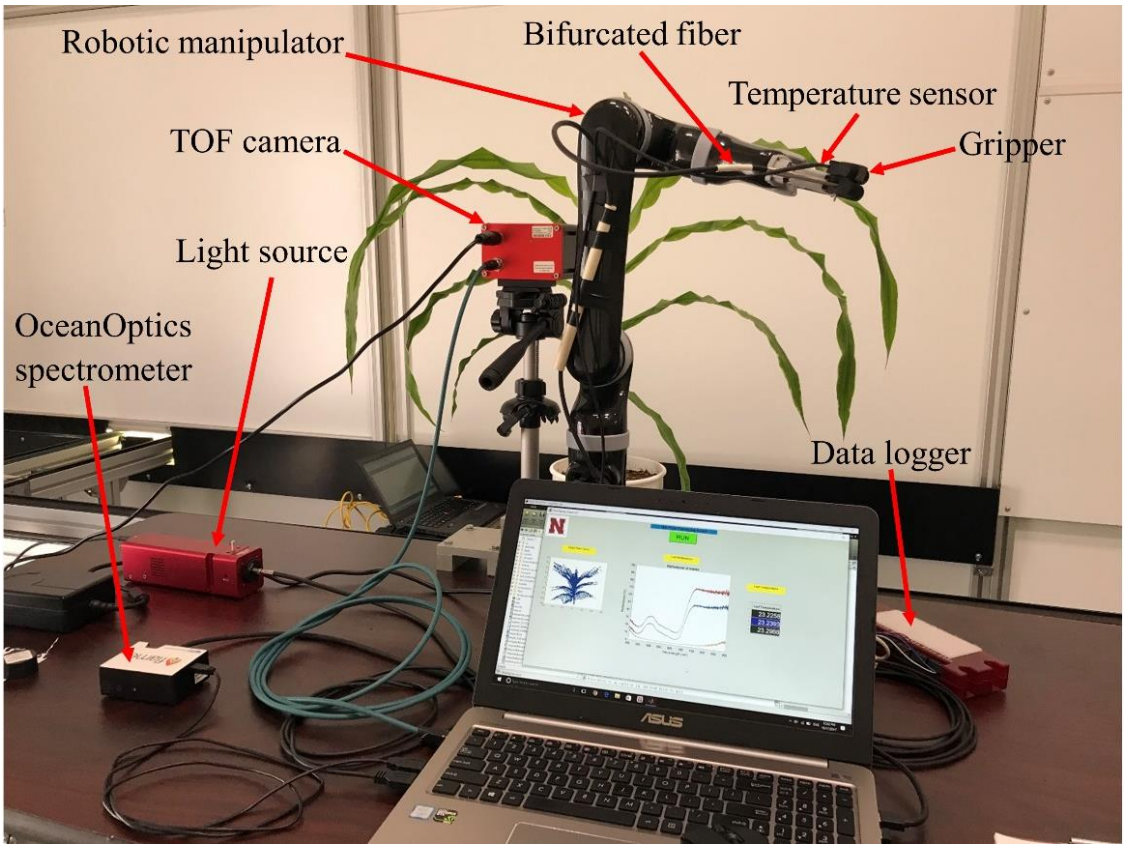

Fig. 2.9. The robotic system and its components

2.2.2 SOFTWARE OF THE ROBOTIC SYSTEM

Image processing for plant segmentation, leaf identification, and grasping point localization: After taking the image using the TOF camera, the Z channel of the scene (plant) was extracted as a grayscale image (Fig. 2.10a). A threshold based on the distance

between the camera and the plant in Z direction was determined to segment the plant from the background, and to create a binary image (Fig. 2.10b).

The even columns of pixels were removed from the binary image. The remaining odd columns appeared as vertical lines in the image as shown in Fig. 2.10c. All vertical lines were labeled. For each vertical line, the coordinates of its center point and its length were determined. Then the length of each line was plotted against its label (Fig. 2.10d). Since the edges of stem have the largest length and cause abrupt changes in the plot, the two abrupt changes and their indices were determined. The indices were used to find the center point of the edges of the stem. The stem was detected using the coordinates of the edges (Fig. 2.10e).

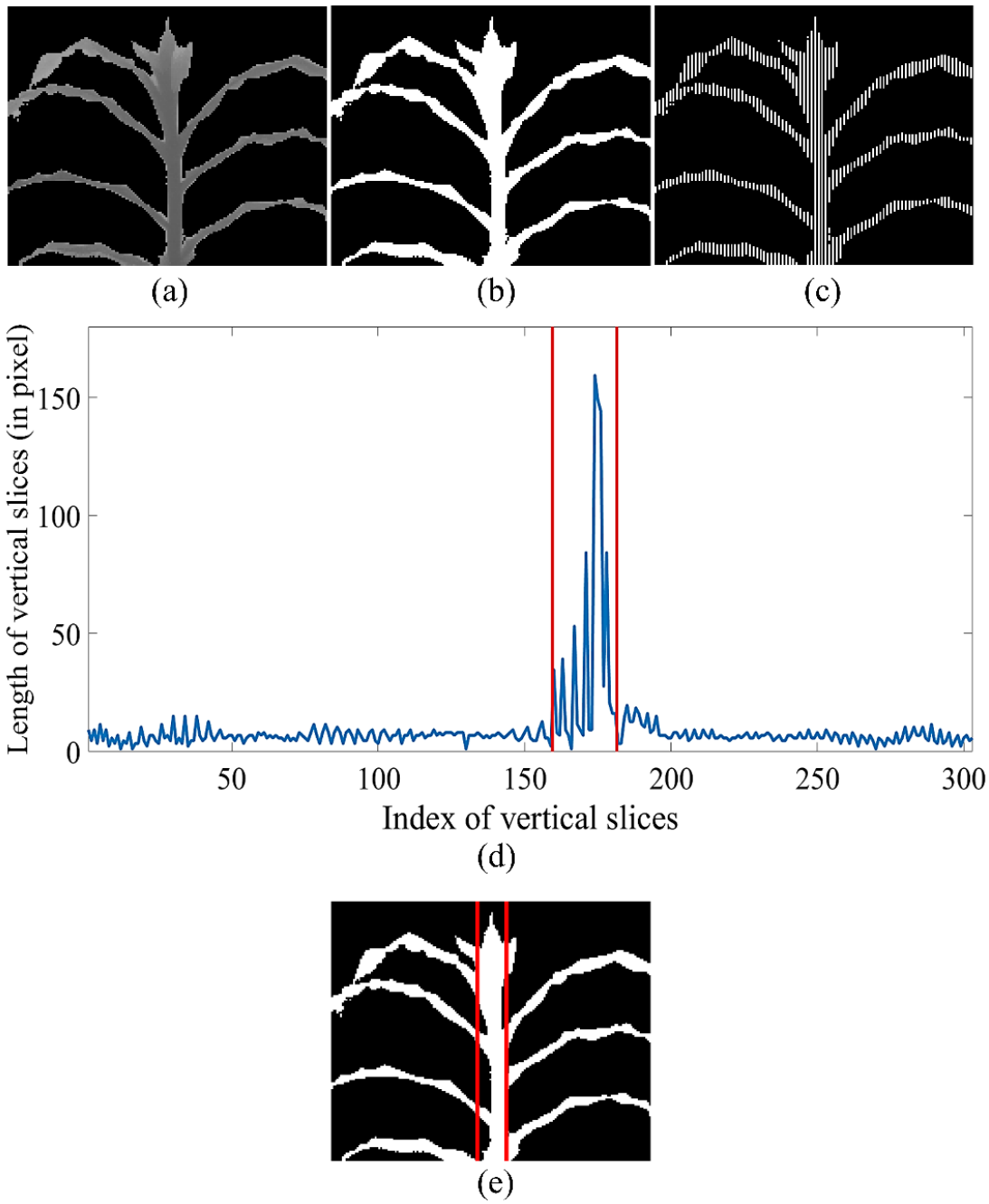

Fig. 2.10. (a) Grayscale image of the plant, (b) Binary image after segmentation, (c) Binary image after removing the even columns of pixels, (d) Major axis length versus the index of the vertical lines, and (e) Stem detection.

The center point of a leaf was chosen to avoid hitting the stem by the robotic manipulator, and also to grasp the leaf properly. After detecting the stem in the image, the

stem was removed and the remaining leaves were labeled. The center point of each leaf along with its 3D coordinates in the camera coordinate system was determined in the binary image as a potential grasping point. A flowchart describing the process of finding the grasping point of the leaves is presented in Fig. 2.11.

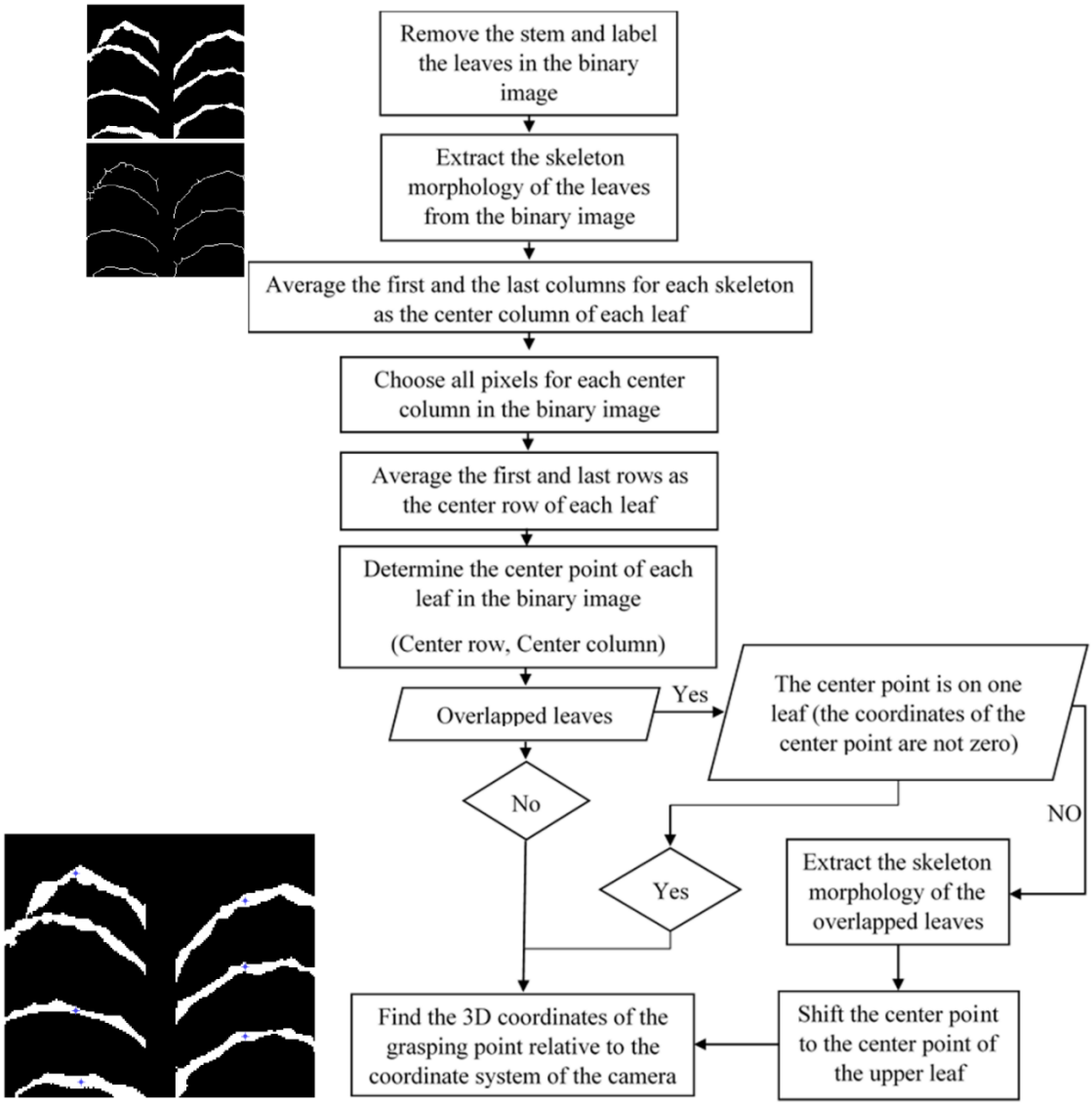

Fig. 2.11. Flowchart for finding the grasping point on the leaves

The leaves were ranked to select the best 3 leaves for measurement (Fig. 2.12). Two criteria were considered to rank the leaves. A leaf having a larger major axis length was

given higher rank because it had greater chance to be grasped by the gripper. Second, a leaf which had shorter distance to the origin of the robotic manipulator's coordinate system was ranked higher in order to reduce the total execution time for the measurement.

The angle of the ranked leaves relative to the horizontal line were determined which in turn was used to calculate the angle of the last joint of the robotic manipulator (fourth joint) to have an appropriate angle for leaf grasping (Fig. 2.12).

The 'regionprops' function in MATLAB returns the sets of properties of connected objects in a binary image. The 'MajorAxisLength' and 'Orientation' properties in 'regionprops' function were used to calculate the length of major axis of each ranked leaf (in pixels) and to compute the angle of the ranked leaves relative to the horizontal line (in degrees).

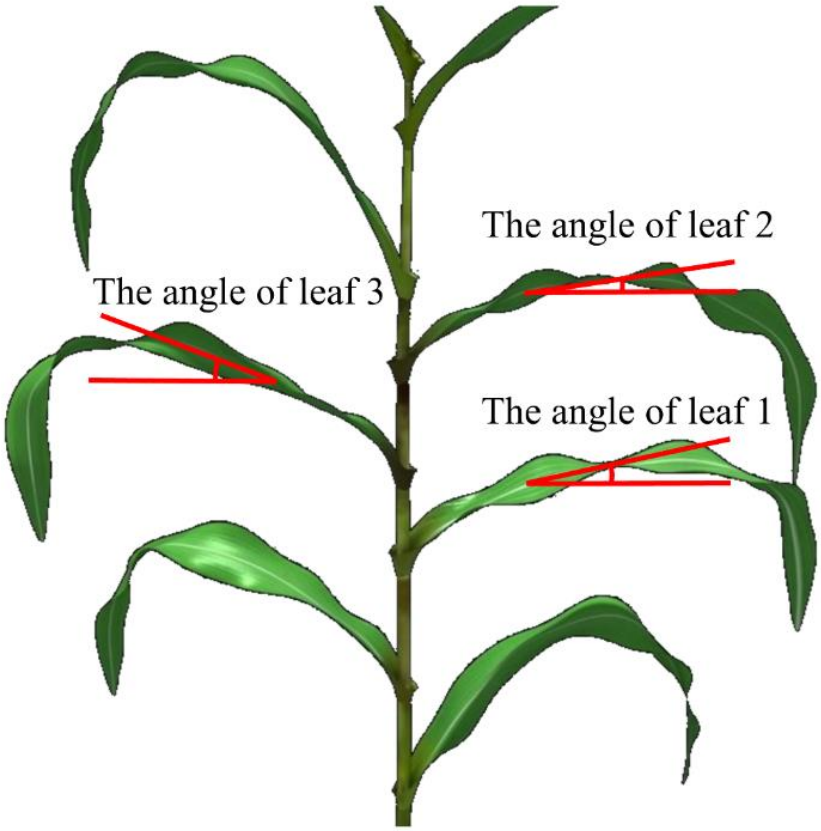

Fig. 2.12. Three best candidate leaves ranked and their angles relative to the horizontal line.

3D plant point cloud: To visualize a 3D model of plant, the 3D point clouds of plant was generated by creating a 3D plot of the plant pixels XYZ coordinates which are provided by the TOF camera (Fig. 2.13).

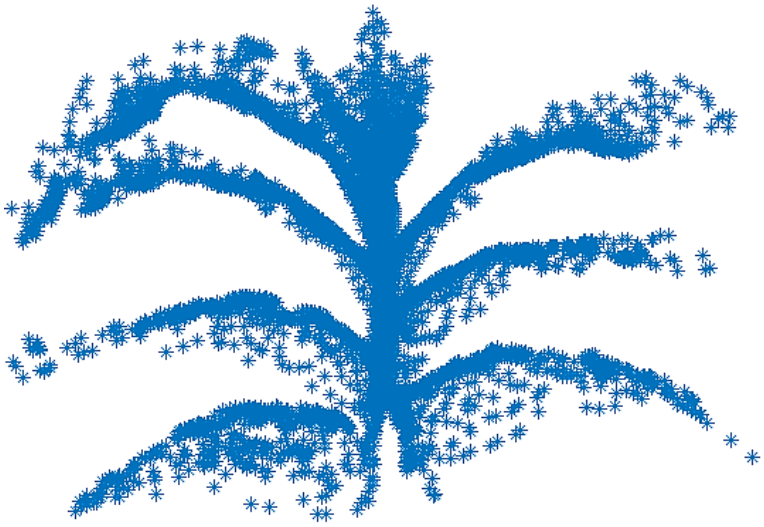

Fig. 2.13. 3D plant point cloud of plant

2.2.3 INVERSE KINEMATICS OF THE ROBOTIC MANIPULATOR

The inverse kinematics was used to compute the set of joint angles of the robotic manipulator given the position and orientation of the end-effector (the position of the grasping point) relative to the base of the robotic manipulator. To reach this purpose, the position of the grasping point in camera's coordinate system was transformed to the robotic manipulator's coordinate system. Then the joint angles were computed using the inverse kinematics in order to grasp the leaf.

The translation from the robotic manipulator's coordinate system to the camera's coordinate system was 10.5 cm, -4 cm, and 41.2 cm in X, Y, and Z directions (Fig. 2.14).

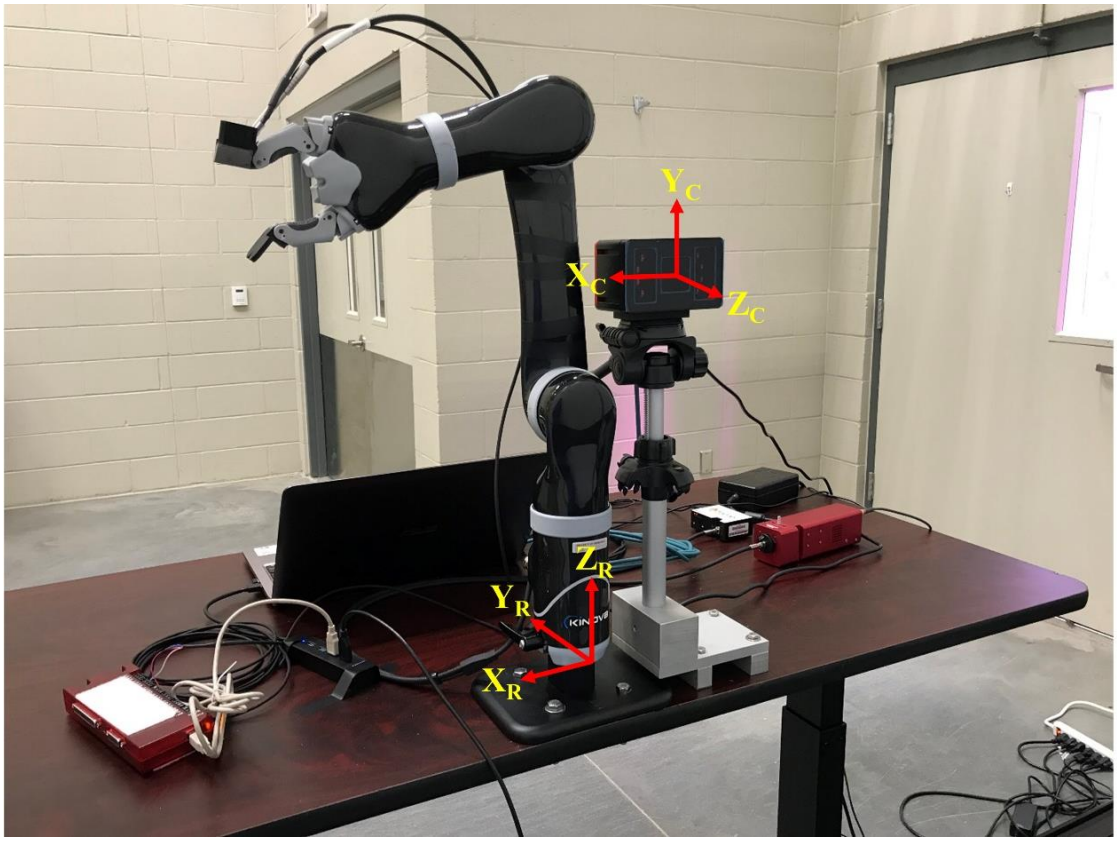

Fig. 2.14. Position of the camera's coordinate system and the robot's coordinate system.

A transformation matrix was determined based on the rotation and the translation of the camera's coordinate system relative to the robotic manipulator's coordinate system (Eq. 2.4).

$$ {}^{R}P = {}^{R}_{C}T \times {}^{C}P \tag{2.4} $$

Where:

$$ {}^{R}_{C}T = \begin{bmatrix} 1 & 0 & 0 & P_x \\ 0 & \cos(90) & -\sin(90) & P_y \\ 0 & \sin(90) & \cos(90) & P_z \\ 0 & 0 & 0 & 1 \end{bmatrix} $$

${}^{R}P$ is the 3D coordinates of the center point of the leaf relative to the robotic manipulator's coordinate system, ${}^{R}_{C}T$ is the transformation matrix between the camera's

coordinate system and the robotic manipulator's coordinate system, ${}^{C}P$ is the 3D coordinates of the center point of the leaf relative to the camera's coordinate system. P_x, P_y, and P_z are the translation from the robotic manipulator's coordinate system to the camera's coordinate system in X, Y, and Z directions. The transformation matrix was used to convert the 3D coordinates of the leaf's center point from the camera's coordinate system to the robotic manipulator's coordinate system (Eq. 2.5-2.7).

$$X_R = X_C + P_x \tag{2.5}$$

$$Y_R = -Z_C + P_y \tag{2.6}$$

$$Z_R = Y_C + P_z \tag{2.7}$$

Where:

X_C, Y_C, and Z_C are the x, y, and z coordinates of the center point of the leaf relative to the camera's coordinate system. X_R, Y_R, and Z_R are the x, y, and z coordinates of the center point of the leaf relative to the robotic manipulator's coordinate system.

The geometric approach was applied to calculate the joint angles of the robotic manipulator. In geometric approach, the spatial geometry of the robotic manipulator is decomposed into several plane-geometry problems. Joint angles are computed using the tools of plane geometry. Two different paths were found based on the inverse kinematics solutions. The path that gave a lower probability of hitting leaves by the robotic manipulator during grasping was chosen (path 1 in Fig. 2.15).

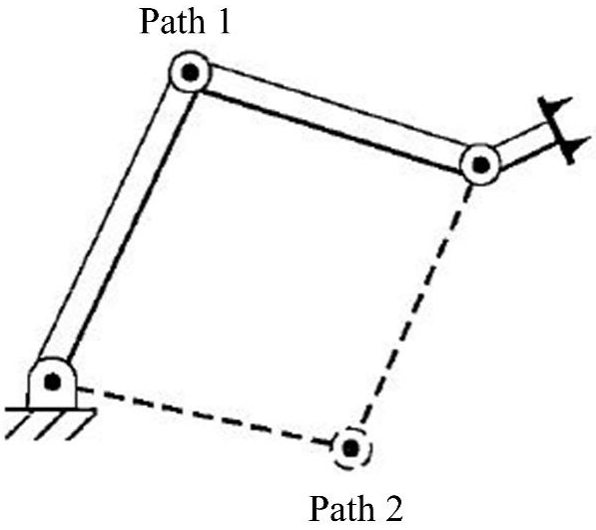

Fig. 2.15. The chosen path (path 1) to grasp the leaf (source: Craig, 2009)

All equations for the inverse kinematics of the robotic manipulator were then derived for the chosen path. The angle of the joints 1 through 4 was calculated using the equations (2.8), (2.10), (2.9), and (2.11), respectively.

$$\theta_1 = atan2(X_R, Y_R) \tag{2.8}$$

$$\theta_3 = atan2(\sin\theta_3, \cos\theta_3) \tag{2.9}$$

Where:

$$\cos\theta_3 = (X_R^2 + Y_R^2 + (Z_R - D_1)^2 - D_2^2 - L^2)/(2 \times D_2 \times L)$$

$$\sin\theta_3 = \sqrt{1 - (\cos\theta_3)^2}$$

$$\theta_2 = atan2(Z_R - D_1, \sqrt{(X_R^2 + Y_R^2)}) - atan2(L \times \sin\theta_3, D_2 + L \times \cos\theta_3) \tag{2.10}$$

$$\theta_4 = (The\ angle\ of\ the\ leaf) + 90 \tag{2.11}$$

Where:

$$L = D_3 + D_4 + D_5$$

The robotic manipulator grasps the ranked leaves in two steps. First, it moves toward the leaf and then stops in an arbitrary distance about 5 cm close to the leaf. Second, it moves horizontally to grasp the leaf (Fig. 2.16). After measuring the leaf reflectance and leaf temperature, the robotic manipulator follows the same path back as in grasping process.

Fig. 2.16. The robotic manipulator grasps the leaf to take measurements

A Graphic User Interface (GUI) was developed in MATLAB (version 2017, MathWorks) to control the portable spectrometer and the thermistor in order to measure leaf reflectance and leaf temperature. The GUI displayed and stored 3D point clouds of the plants (from the TOF camera), the VisNIR reflectance of the leaves, and leaf temperature readings (Fig. 2.17). The GUI also integrated the image processing algorithm and inverse kinematics calculation as described above. It stored the times for image processing, inverse kinematics calculation, leaf approaching and grasping, sensing process, and the total execution time which was the time that the robotic system accomplished the entire task.

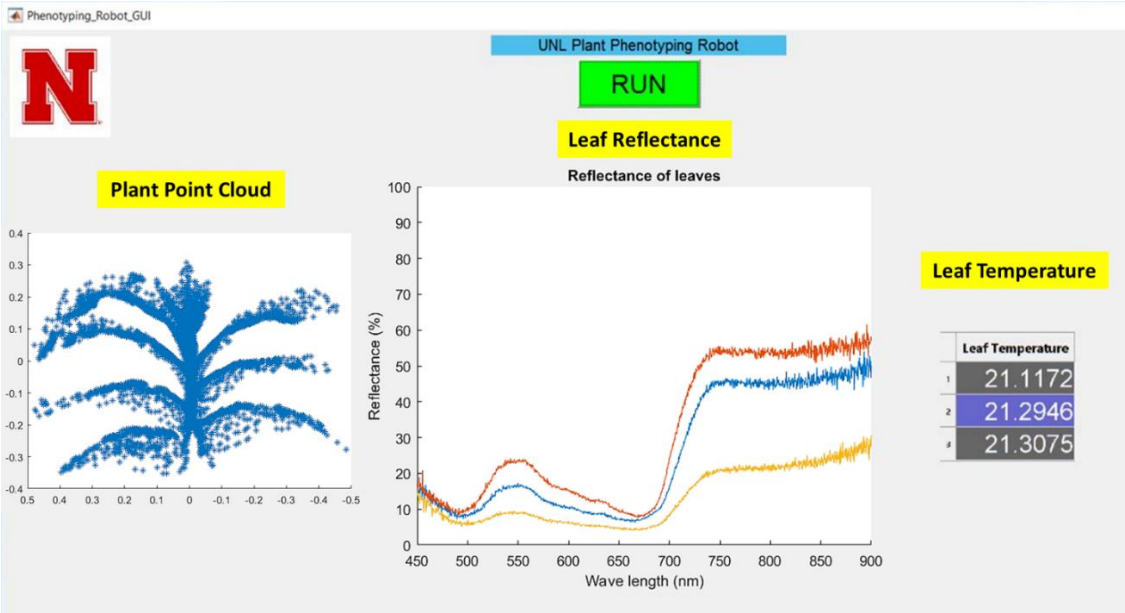

Fig. 2.17. The graphic user interface developed in MATLAB to control the plant phenotyping robot and display the robotic measurements.

2.2.4 TESTING AND DATA ANALYSIS

To test the function and performance of the phenotyping robot, an experiment was conducted in the Greenhouse Innovation Center of the University of Nebraska-Lincoln.

This greenhouse was equipped with a high-throughput plant phenotyping system (Scannalyzer3D, LemnaTec GmbH, Aachen, Germany). During test, the robotic system was emplaced alongside the system's conveyor belt. Plants were loaded onto the conveyor belt and transported to the system for robotic phenotyping (Fig. 2.18). The distance between the camera and the plants was 20~30 cm.

Fig. 2.18. The emplacement of the robotic system in the greenhouse

Sixty maize (B73) and sixty sorghum plants (TX430) were grown in the pots and used to evaluate the robotic system (Fig. 2.19). The experiment included two levels of water treatment (well-water versus water-limitation) and two levels of applied nutrients (high versus low). Each plant was randomly assigned to one of the four treatment combinations, and the goal was to create a large variation in plant leaf properties

(reflectance spectra and temperature) to validate automated robotic measurements. The well-water treatment was achieved by watering pots to 80% of field capacity on a daily basis, while the water-limitation treatment 40% of field capacity. The high-nutrient treatment was achieved by adding 0.122 kg of Osmocote Plus fertilizer (15-9-12 (N-P-K) with micronutrients, 3-4 months nutrient release) into pot mix (5.67 L) at the time of planting. For low nutrient level, fertilizer liquid with 100 ppm concentration of 20-10-20 (N-P-K) fertilizer with micronutrients were added.

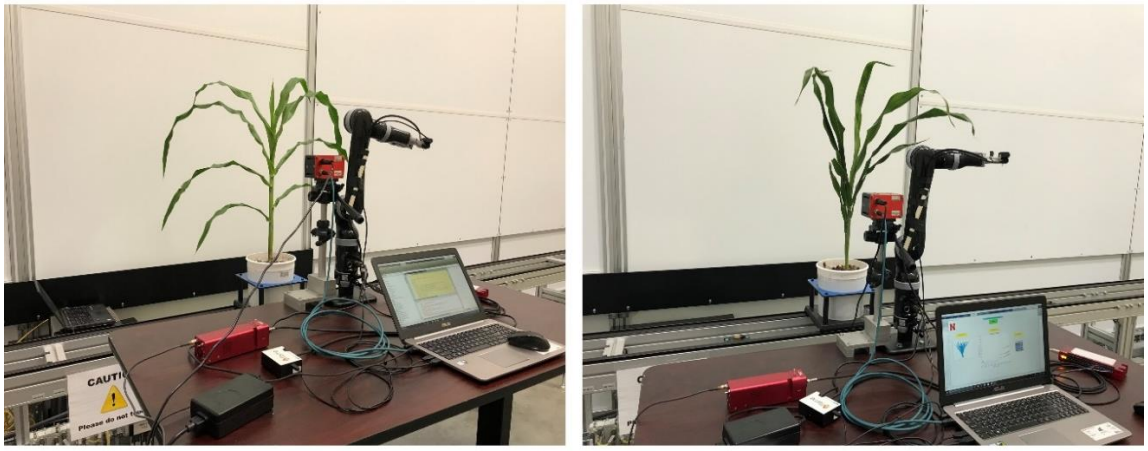

Fig. 2.19. Maize B73 (left) and sorghum TX430 (right)

Data collection started when the plants were at nine leaf stage and lasted until the plants were at 13 leaf stage. The experiment was done in six weeks. Five days were chosen in each week for data collection; and in each day, data were collected from four plants with different combination of water and nutrient treatments.

Immediately after robotic phenotyping, ground-truth measurements (manual measurements by a researcher) were taken to compare with automated robotic measurements (automated measurements). A spectroradiometer (Model: FieldSpec4, Analytical Spectral Devices Inc., Longmont, CO, USA), a thermistor (Model: ST 200:

Fine-Wire Thermistor, Apogee Instruments Inc., Logan, UT, USA), and a handheld chlorophyll meter (Model: MC-100 Chlorophyll Concentration Meter, Apogee Instruments Inc., Logan, UT, USA) were used to measure leaf reflectance, leaf temperature, and leaf chlorophyll content at the grasping points (Fig. 2.20). For each plant, up to three ground-truth and automated robotic measurements (from three grasping points identified by the robots) were made. They were averaged to represent the measurements for that plant.

Fig. 2.20. Ground-truth measurements by a researcher: leaf reflectance spectrum (left), leaf temperature (middle), and leaf chlorophyll content (right).

After the automated and ground-truth measurements, the plant was harvested and the fresh weight of aboveground biomass was recorded. After drying the plant for 72 hours at 50 $^{\circ}$C to constant dry weight, leaf water content was calculated. The dried leaves of the plant were sent to a commercial lab (Midwest Laboratories, Omaha, NE, USA) and leaf Nitrogen (N), Phosphorus (P), and Potassium (K) concentrations were measured.

For the VisNIR spectra from the Ocean Optics spectrometer (robotic measurements), a range from 450 to 950 nm was used (to avoid high noise regions at the two ends of spectra) for modeling and predicting leaf chemical properties. Spectra were smoothed with a moving average window (of size 30) to further reduce the noise of spectra.

Similarly, spectra from the ASD spectrometer were also truncated between 450 and 950 nm for modeling and prediction. Partial least squares regression (PLSR) models of different leaf properties were calibrated using the spectra with six random segment cross-validation (60% for cross-validation and 40% for validation). Data analysis was performed in R Statistical Software (R Core Team, 2017) with the following packages: pls (Mevik et al., 2016), caret (Kuhn et al., 2017), and zoo (Zeileis and Grothendieck, 2005).

Two different success rates were defined and calculated for the robotic system in order to assess its performance to grasp leaves and collect data in the greenhouse.

1) The integration success rate: It was defined as grasping at least one leaf per plant and record the measurements successfully before releasing the plants from the robotic station.
2) The grasping success rate: It was defined as the ratio between the number of the leaves which were successfully grasped and the total number of the leaves identified as the candidate grasping leaves.

2.3 RESULTS AND DISCUSSIONS

2.3.1 THE PERFORMANCE OF THE ROBOTIC SYSTEM

Table 2.2. Summary statistics for the execution time of different steps in automated robotic measurement of one leaf.

Time (s)	Statistic	Maize plant	Sorghum plant
Image processing	Maximum	3.86	4.30
	Minimum	2.32	1.89
	Average	3.05	2.64

	Standard deviation	0.412	0.470
Inverse kinematics	Maximum	0.049	0.060
	Minimum	0.016	0.013
	Average	0.026	0.026
	Standard deviation	0.009	0.009
Leaf grasping	Maximum	45.5	45.1
	Minimum	22.5	22.2
	Average	31.5	33.6
	Standard deviation	5.17	5.79
Sensing process	Maximum	2.44	1.75
	Minimum	0.845	0.858
	Average	1.19	1.24
	Standard deviation	0.356	0.344
Total execution	Maximum	47.2	52.9
	Minimum	30.3	29.2
	Average	35.5	38.5
	Standard deviation	4.39	5.68

Table 2.2 gives summary statistics of the execution time for image processing, inverse kinematics, leaf grasping, sensing process, and total execution time to measure one leaf for maize and sorghum plants. Leaf grasping, which involved bringing the robotic gripper and sensors into contact with the leaves, took the longest time to execute. Image processing was computationally more intensive than inverse kinematics and thus took longer to execute.

The execution times for different steps and total execution time were comparable for maize and sorghum plants, and it was approximately 30 s to take one robotized measurement. This was significantly longer than human based measurement, which only took 5-6 s in our case.

The image processing to segment the leaves from the stem worked well for maize plants. However, the specific variety of sorghum we chose to work with (TX430) exhibited more vertically distributed leaves than maize. This sorghum morphology made it more challenging to remove stem pixels while retaining leaf pixels for leaf identification and grasping point localization (Fig. 2.19). For this reason, the integration success rate was only 48% for sorghum plants, much lower than 78% for maize plants.

The grasping success rate for maize plants was 50% and that for sorghum plants was similar (~50%). The experiment also showed that the phenotyping robot could grasp on average two leaves per plant and collect data successfully. It failed to grasp a leaf for three main reasons. First, if the 3D coordinates of the grasping point were out of the workspace of the robotic manipulator, the robotic manipulator was not driven to grasp the leaf. Second, since the camera had uncertainty to measure the z coordinate of the scene (±2 cm), it could cause an error in the calculation of the joint angles of the robotic manipulator and only grasped the target leaf partially at the edge of the leaf. Third, if the leaf was vertical (i.e. approximately 90° angle from the horizontal plane), the manipulator could not grasp the leaf due to the lack of needed dexterity and degree of freedom.

Fig. 2.21 compares the leaf temperature of maize and sorghum plants measured by the human operator (ground-truth) with that measured by the phenotyping robot. It can be seen that two sets were linearly correlated (R^2 = 0.58 for maize plants, R^2 = 0.63 for sorghum, and R^2 = 0.62 for maize and sorghum plants together). However, there was also significant bias between them. Robotized temperature measurement was 0.71 $^{\circ}$C lower than the manual measurement in maize, 0.81 $^{\circ}$C lower in sorghum, and 0.76 $^{\circ}$C in both species together. Three factors could be attributed to the bias between the two

temperature measurements. Firstly, when the human operator took the temperature measurement, she always ensured good contacts between the leaf and the sensor. This was quite challenging for our phenotyping robot, which lacked the needed dexterity, degree of freedom, and the sense of pressure to orient its manipulator and gripper perfectly with the leaf surface to have a good contact. This could explain the negative bias of the robotized measurements. The second factor could be due to the fast change of leaf temperature relative to ambient temperature. There were large temperature differences between the greenhouse (where the plants were grown) and the head house (where the measurements were taken). Leaf temperature was likely not in a steady state during measurement. There was a slight time difference between the manual and robotic measurement, which would lead to small bias between the two sets of temperature measurements. Thirdly, the two temperature sensors used by the human operator and the phenotyping robot were not cross calibrated. They could indicate a temperature different as large as 0.5 °C even when they were to measure the same object; and the sensor used by the human operator were known to indicate slightly higher temperature.

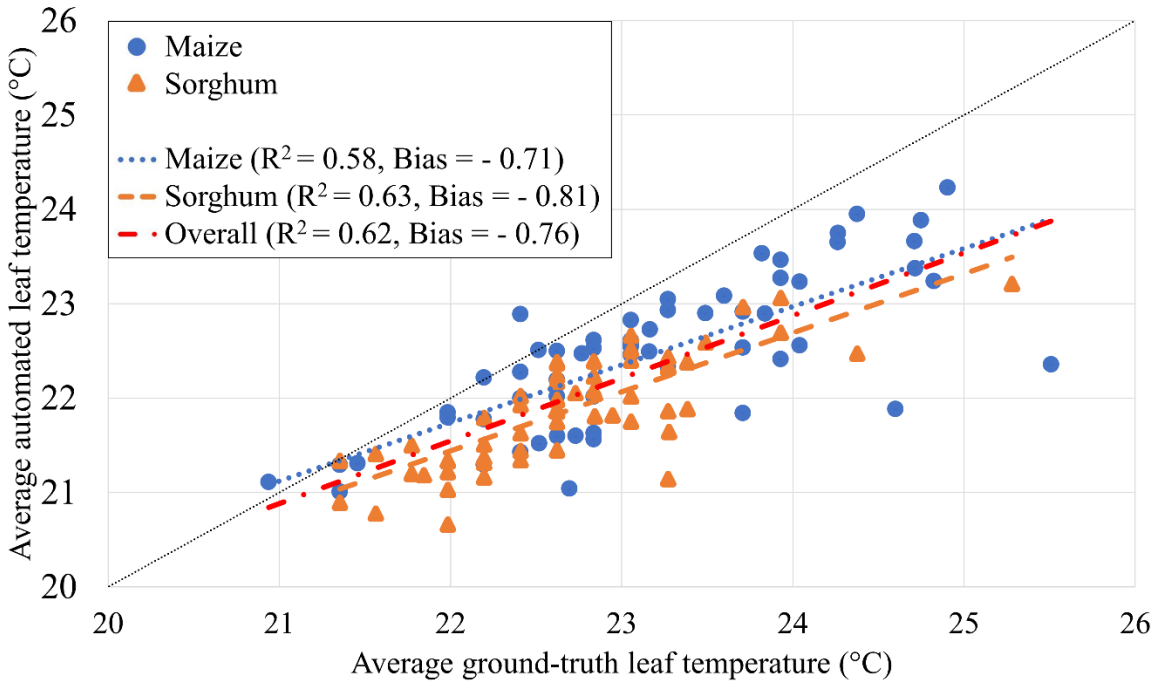

Fig. 2.21. Scatterplot of leaf temperature measured by the human operator versus the phenotyping robot for maize and sorghum plants. The linear regression and the statistics were reported for maize, sorghum, and the two species together.

We further conducted a Welsh's two-sample t-test to compare leaf temperature of the plants under the two water treatments. The rationale for this comparison was that the plants under the water limitation treatment should exhibit higher leaf temperature due to the drought effect of reduced leaf-level transpiration (Fig. 2.22). The results showed that, for maize plants, leaf temperature was significantly higher (p-value = 0.018) when measured manually by the human operator. However, such difference was not significant (p-value = 0.111) for the automated robotic measurements, even though the mean temperature for the water limitation group was slightly higher. For sorghum, neither manual measurements nor robotic measurements exhibited significant difference between the two water treatment groups (p-values = 0.245 and 0.068, respectively). Sorghum is

more drought tolerant than maize, which could explain although there is still improvement to make robotized leaf temperature measurements more accurate, this comparison suggested one potential use of our phenotyping robot to distinguish drought-tolerant lines from drought-sensitive lines.

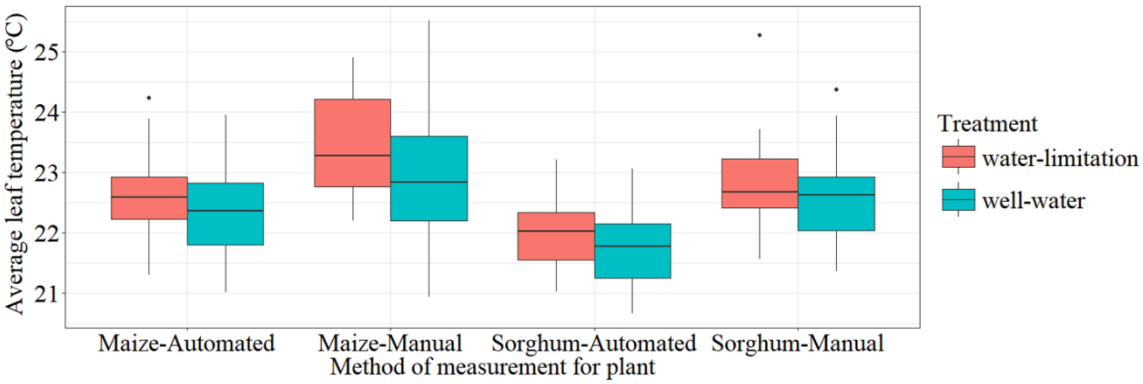

Fig. 2.22. The box plots of average manual and automated leaf temperatures for maize and sorghum with two water treatments

2.3.2 CHEMOMETRIC PREDICTION OF LEAF CHEMICAL PROPERTIES FROM LEAF REFLECTANCE DATA

Table 2.3 gives results of PLSR modeling of leaf chemical properties using leaf reflectance spectra measured by the phenotyping robot in comparison to manual measurements. Among the five leaf properties studied, leaf chlorophyll content was predicted most successfully, followed by fresh-based water content and K. Prediction of N and P exhibited poorer performance. Fig. 2.23 shows the scatterplots of predicted versus measured leaf properties in maize and sorghum for both manual and robotic measurements.

The predictions with spectra data from the ASD spectrometer were substantially better than with those from the OceanOptics spectrometer. Note that ASD spectra were

acquired with a human operator, whereas OceanOptics spectra were acquire automatically with the phenotyping robot. During spectral data collection, the human operator always ensured that the leaf clip was in close contact with the leaf. In many occasions, she was using the other hand to guide the orientation of the leaf blade such that no light was leaked out of the measurement point. This was very difficult to achieve with our phenotyping robot due to poor contact between the gripper and leaf reducing the light throughput of the signal. This resulted light leakage and thus lower spectral quality in leaf reflectance measurement.

Table 2.3. Results of partial least squares modeling to predict leaf chemical properties using leaf reflectance spectra measured by the phenotyping robot in comparison to manual measurements.

Property	Manual						Robotic					
	Cross-validation			Validation			Cross-validation			Validation		
	R^2	RMSE	Bias	R^2	RMSE	Bias	R^2	RMSE	Bias	R^2	RMSE	Bias
CHL ($\mu mol/m^2$)	0.907	57.9	0	0.865	69.0	-11.0	0.664	119	0	0.525	112	-1.12
FBWC (%)	0.891	1.97	0	0.861	2.25	0.517	0.637	3.46	0	0.614	3.75	1.12
N (%)	0.602	0.271	0	0.384	0.333	-0.078	0.421	0.331	0	0.139	0.374	-0.036
P (%)	0.567	0.112	0	0.565	0.114	-0.003	0.406	0.139	0	0.112	0.230	-0.063
K (%)	0.870	0.500	0	0.788	0.667	-0.027	0.693	0.835	0	0.519	1.00	0.020

CHL= Chlorophyll content, FBWC = Fresh-based water content, N = Nitrogen, P = Phosphorus, K = Potassium, RMSE = Root mean squared error

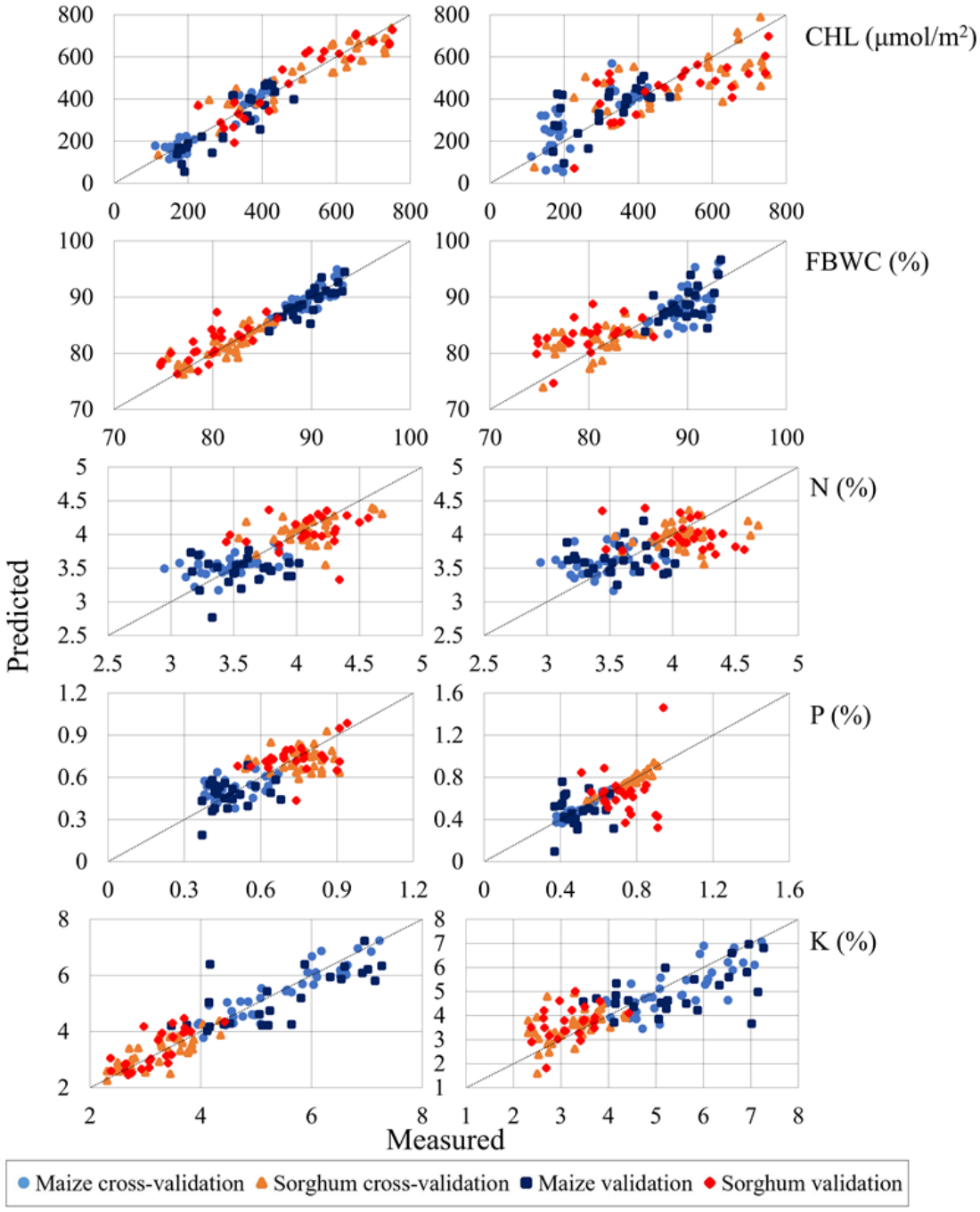

Fig. 2.23. Scatterplots of lab-measured versus predicted leaf properties of maize and sorghum plants for manual measurement (left column) and robotic measurement (right column).

2.4 POTENTIAL IMPROVEMENTS AND FUTURE DIRECTIONS

We developed and demonstrated a robotic system that can realize *in vivo*, human-like measurements of plant leaf traits in the greenhouse. This approach is different from the traditional image-based phenotyping, where plant images are used as a nondestructive means to acquire predominantly morphological traits such as height, width and projected leaf area. Even though some imaging modules such as NIR and hyperspectral imaging can probe leaf biochemical traits (Pandey et al., 2017), they still need manual measurements to establish correlations with image data. In this sense, the phenotyping robot would be useful to complement image-based phenotyping by obtaining physiological or chemical measurements at the plant leaf level.

We integrated to the robotic gripper a fiber optical cable to measure leaf-level reflectance and a thermistor to measure leaf temperature. With some mechanical modifications, sensors to measure other leaf properties (such as stomatal conductance, gas exchange, chlorophyll content, etc.) can be integrated. It is also possible to integrate a mechanical sampler to cut and collect leaf disks with the robotic gripper. While the measurement speed of the phenotyping robot is slower than that of a human operator, many of these robots (equipped with different plant sensors) can be launched in the greenhouse, which would substantially enhance the speed and capacity of the phenotyping robot. Furthermore, many modern greenhouses already have conveyor systems to move the plants around, which would make the integration of the phenotyping robots with the existing greenhouse infrastructure straightforward.

The phenotyping robot realized its designed functions of automated leaf probing and leaf-level trait measurement. Its performance, nevertheless, could be further improved.

Firstly, a robotic manipulator with more degree of freedom would make the robot more dexterous and flexible to probe the leaves. This measure would ensure good contact between the gripper/sensors and plant leaves, which is critical to improve quality of sensor measurements. Secondly, a collision free path planning algorithm would be designed and implemented. This technique finds the optimal path for the robotic manipulator's movements between two grasping points without hitting the leaves or stem and potentially reduces execution time. Thirdly, the TOF camera we used is low in spatial resolution and introduces large uncertainties in determining the XYZ coordinates of grasp points. Using a range camera with higher accuracy can improve grasp point localization, and therefore improve the overall success rate of leaf probing and robotic measurements. Finally, the test plants were all placed with their symmetrical plane facing the TOF camera. In this position, leaf occlusion was minimized which was instrumental to subsequent image processing and robotic measurements. In real applications, plants would be randomly oriented and presented to the imaging system, therefore causing a number of problems regarding leaf segmentation and robotic measurements. These challenges need to be sufficiently tested and addressed for real life applications.

2.5 CONCLUSIONS

In this research, we designed and developed a plant phenotyping robotic system to realize *in vivo*, human-like leaf trait measurement. The system comprised of a 3D TOF camera, a four DOF robotic manipulator, and a custom-made gripper that integrated a bifurcated fiber optic cable and a thermistor. This robotic system was tested in the greenhouse using maize and sorghum plants. The test result showed moderate accuracy for measuring several leaf traits including temperature, chlorophyll content, fresh-based

water content, and potassium (R^2 ranged from 0.52 to 0.62) by the phenotyping robot in comparison to the ground-truth measurement. The leaf grasping success rate was ~50% for both maize and sorghum, and the average execution time to take measurements from one leaf was 35.5 s for maize and 38.5 s for sorghum. To collect leaf properties data using the robotic system, the researcher does not need to hold different sensors for data collection. The researcher just needs to run the program and the system automatically gathers the phenotypes. Therefore, the robotic system no longer needs a human for collecting phenotypic data and consequently the system could remarkably decrease the tedious nature of data collection. This phenotyping robot has a potential to complement image-based high throughput plant phenotyping by measuring leaf physiological and chemical traits directly and automatically.

CHAPTER 3

AN AUTOMATED ROBOTIC SYSTEM TO MEASURE STEM DIAMETER OF MAIZE AND SORGHUM PLANTS IN GREENHOUSE

3.1 INTRODUCTION

Plant phenotyping is a key technology for the crop breeders to produce plants with desirable traits such as higher yield, disease resistance, and drought tolerance (Mueller-Sim et al., 2017). It assesses the quantitative measurements of crop phenotypes such as leaf area, leaf angle, and stem diameter (Schepers et al., 2017). The stem diameter of a plant is a good indicator to judge about the plant's health and predict the crop yield. A plant which has a thicker stem diameter is usually considered as healthier plant with higher yield potential than other plants at the same growth stage (Shi, 2014). However, the manual measurements of this phenotype (stem diameter) is laborious, time consuming, tedious, and error prone (Baweja et al., 2018). Robotic phenotyping will be able to help geneticists to investigate the interaction between genotype and phenotype more easily in order to improve the crop yields (Mueller-Sim et al., 2017).

A prototype-sensing device which consisted of a laser light source and detector, and also simulation apparatus was developed for automated measurement of maize stem diameter (Schepers et al., 2017). The system enabled to measure the stem diameter accurately in the laboratory. Shi (2014) developed two on-the-go approaches based on machine vision technique to measure stem diameter of maize. Both approaches had an acceptable performance to measure the stem diameter. Vázquez-Arellano et al. (2018)

developed a method to estimate the position and height of the maize stem from 3D reconstruction of the plant using the point cloud data of a TOF camera. The experimental results showed that their method could determine the position and height of the stem with an average mean error of 24 and 30 mm. Chaivivatrakul et al. (2014) developed an automated plant phenotyping system which could measure morphological trait characterization for maize plants via 3D holographic reconstruction. A TOF camera and a rotating table were used to acquire point cloud image data. Their proposed method could able to create accurate 3D holographic reconstruction of maize, and also showed promising results to segment leaf and stem, and measure the plant phenotypic data such as stem major axis, stem minor axis, and stem height. Jin et al. (2019) proposed a median normalized-vector growth (MNVG) algorithm which could segment leaf and stem, and also extract phenotypic traits of leaf, stem, and individual maize plant such as leaf area, stem diameter, and plant height using terrestrial LiDAR data. They tested their algorithm for maize plants with different height and leaf numbers with three growing stages. The experimental results showed that MNVG method had high accuracy for phenotypic traits extraction at individual level (R^2 could be up to 0.96), following by at leaf and stem levels. Das Choudhury et al. (2017) developed an algorithm to automatically compute the angel of maize stem which is a potential measure for plant's susceptibility to lodging. A graph theoretic approach was applied to recognize leaf-tips and leaf-junctions from visible light image. A regression line curve was fitted to the leaf junctions to form the stem axis, and the angle between the stem axis and the vertical axis was determined as stem angle. Their method was tested on Panicoid Phenomap-1 dataset and an accuracy of 84% was achieved.

Deep learning is an emerging area of machine learning which has been proposed as a future trend in image-based plant phenotyping (Tsaftaris et al., 2016). Jin et al. (2018) used deep learning and regional growth algorithms for individual maize segmentation from terrestrial LiDAR data. They used Faster R-CNN model (deep learning) to detect the maize stem. The detected stem seed points were used by the regional growth algorithm to segment the individual maize. The experimental results showed that the method had promising results for maize segmentation from LiDAR data. Baweja et al. (2018) developed a method based on deep learning technique (Faster R-CNN and semantic segmentation) to extract stem count and stem diameter of maize in the field. They compared the automated measurement with manual measurement (ground-truth) in order to validate the accuracy and efficiency of their method. The results showed that the automated measurement for stem count had correlation with manual measurement with R^2=0.88 and the mean absolute error to measure stem diameter was 2.77 mm where average stalk width is 14.354 mm. The automated measurement was 30 and 270 times faster than manual measurement for stem count and stem diameter measurement.

Lu et al. (2017) developed an automated robotic phenotyping platform for corn seedling morphological traits characterization. A TOF camera was attached to the end-effector of a robotic manipulator. The camera was positioned in different views by the robotic arm in order to obtaining 3D point cloud data of the plant. The robotic system could satisfactorily segment the stem and leaves and also measure the stem height and leaf length of corn seedlings. Mueller-Sim et al. (2017) developed a high-throughput ground based agricultural robot which could able to navigate between sorghum rows in the field and collect plant phenotypic data autonomously. The robot used a mobile

platform, a three DOF manipulator, a customized gripper consisted of a digital force gauge and a needle at the end of its probe to measure the stem strength, and non-contact sensors such as a stereo camera to gather phenotypic data. The results of outdoor experiments showed that the algorithm for stem detection worked well and all identified stems were grasped by the gripper successfully.

The objective of this study was to develop an automated plant phenotyping robotic system which could measure the stem diameter of maize and sorghum plants in greenhouse less tediously compare to manual measurements. The performance of the robotic system was evaluated by conducting a validation experiment in the greenhouse.

To the best of our knowledge, this research proposed the first contact-based and non-destructive plant phenotyping robotic system which could automatically measure the stem diameter in real-time. This system could be a complement for image-based high-throughput plant phenotyping. Moreover, contact-based sensors could be later added to this system to measure other physiological and chemical attributes of the stems.

3.2 MATERIALS AND METHODS

3.2.1 HARDWARE OF THE ROBOTIC SYSTEM

Vision system: A TOF camera (Model: SR4500, Mesa Imaging Inc., Zürich, Switzerland) was used to take image from plant. The camera has 176×144 resolution with 69°×55° field of view. XYZ (three channels) coordinates of each pixel in the image relative to the center of camera coordinate system are provided by the camera. A grayscale image can be created using each channel of the image.

Robotic manipulator: A four DOF robotic manipulator (Model: MICO2, KINOVA Inc., Boisbriand, Quebec, Canada) was used in the robotic system.

Gripper: A gripper was designed to attach a linear potentiometer (LP) for stem diameter measurement. Fig. 3.1 shows the 3D sketch of the gripper. The design of the gripper prepares linear and parallel movement for the claws which allows the LP sensor for linear displacement measurement. The gripper was made of plastic to reduce its weight and printed by a 3D-printer.

Fig. 3.1. The 3D sketch of the robotic gripper

Sensing system: A linear potentiometer (Model: LP804-03, OMEGA Engineering Inc., Norwalk, CT, USA) was attached to the gripper to measure the stem diameter (Fig. 3.2). The linear potentiometer has 28 g weight and it can measure linear displacement up to 76 mm with resolution of 0.00127 mm. A data logger (Model: LabJack U6, LabJack Corporation, Lakewood, CO, USA) was used to collect the data taken by the linear potentiometer.

The linear potentiometer was calibrated using a digital caliper to convert the output voltage of the linear potentiometer to linear displacement (stem diameter). Eq. 3.1 shows the calibration equation of the linear potentiometer.

$$d = 0.5817 \times V_{OUT} \tag{3.1}$$

Where:

d is the linear displacement (stem diameter) in inch and V_{OUT} is the output voltage of the linear potentiometer in V.

The linear displacement in inch (d) can be converted to linear displacement in cm (D) using Eq. 3.2.

$$D = 2.54 \times d \tag{3.2}$$

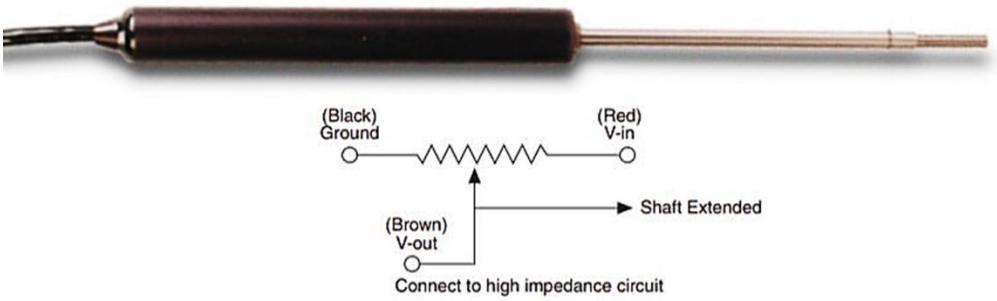

Fig. 3.2. The linear potentiometer and its schematic diagram (source: OMEGA Engineering, 2018)

A microcontroller (Model: Arduino UNO ATmega328 board) together with a dual H-bridge motor driver (Model: Qunqi L298N) was used to control a low-power DC motor (Fig. 3.3). The brushed gear DC motor (Model: 47:1 Metal Gearmotor, Pololu Corporation, Las Vegas, NV, USA) with a 47:1 gearbox and a 48 CPR (counts per

revolution) quadrature encoder was used to open and close the gripper's claws for stem grasping process (Fig. 3.4). Fig. 3.5 shows the schematic diagram to control the DC motor using the microcontroller and motor driver.

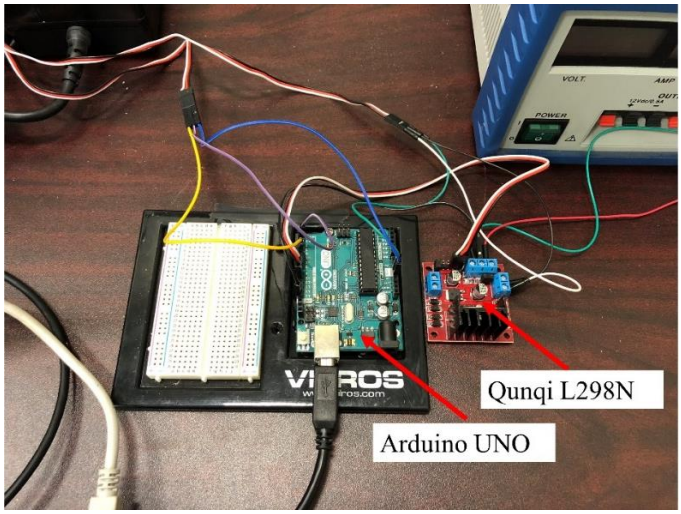

Fig. 3.3. The microcontroller Arduino UNO and motor driver Qunqi L298N

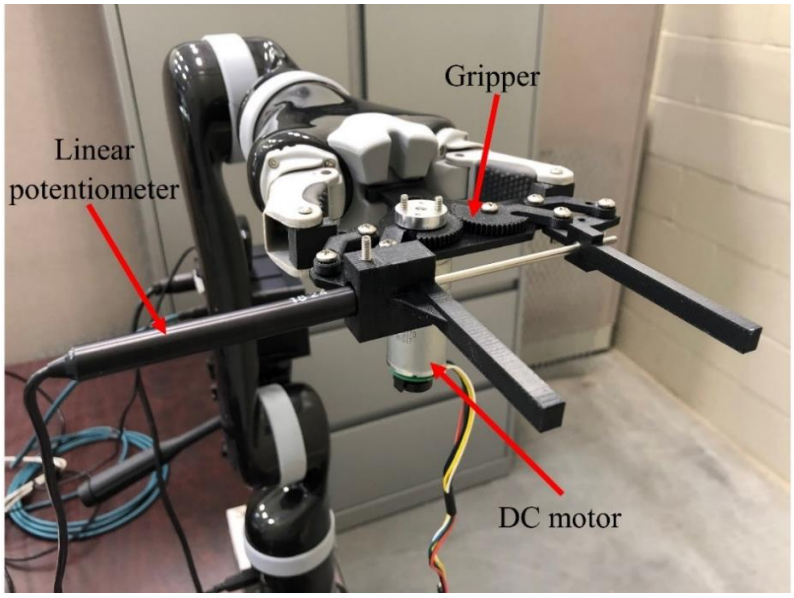

Fig. 3.4. Gripper, Linear potentiometer, and DC motor

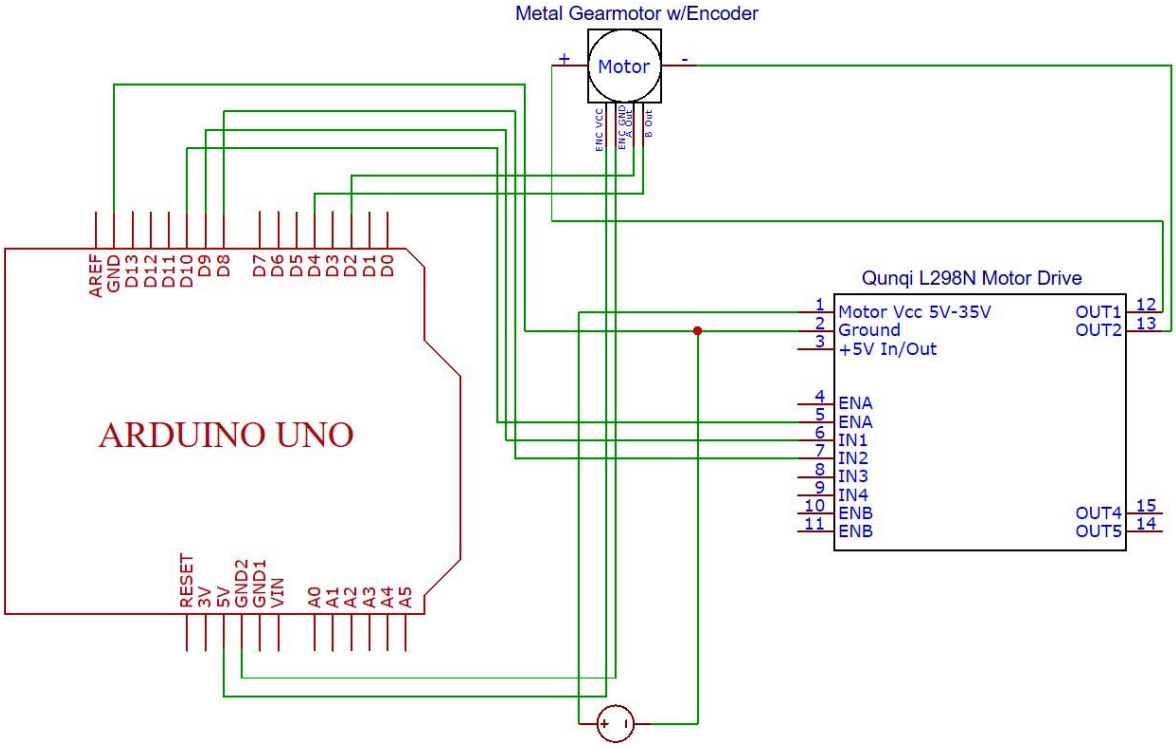

Fig. 3.5. Schematic diagram to control the DC motor

Integration of the robotic system: The camera was installed near the robotic manipulator. The linear potentiometer and the DC motor were attached to the gripper. To adjust the robotic system with the height of the plants, all components were mounted on the top of a height adjustable desk (Fig. 3.6).

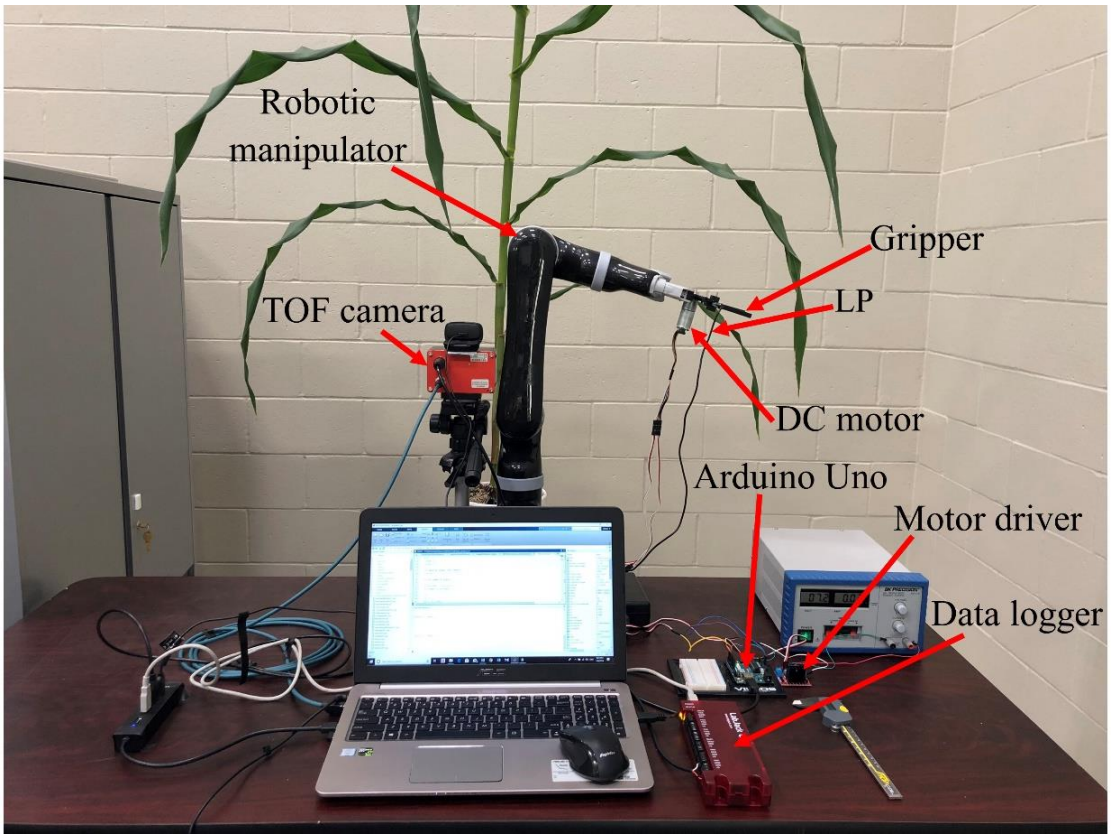

Fig. 3.6. The robotic system and its components

3.2.2 SOFTWARE OF THE ROBOTIC SYSTEM

Stem detection using deep learning technique (Faster R-CNN): Sixty gray-scale images (the images from the TOF camera) were used as the raw data set. The images were labeled using ImageLabeler toolbox in MATLAB (version 2018, MathWorks). Image augmentation technique was used to produce more images for training the network. To reach this goal, the images were sharpened, blurred, darkened, and

brightened (Fig. 3.7). 240 images were produced after applying the augmentation technique and in total 300 images were used as data set. Since the size of data set was small even after applying image augmentation, the data set was split to two subsets: 80% (240 images) as the training set and 20% (60 images) as the testing set. The training dataset was used to train the model and find the weights and biases of the network, and the testing dataset was used to evaluate the performance of the network.

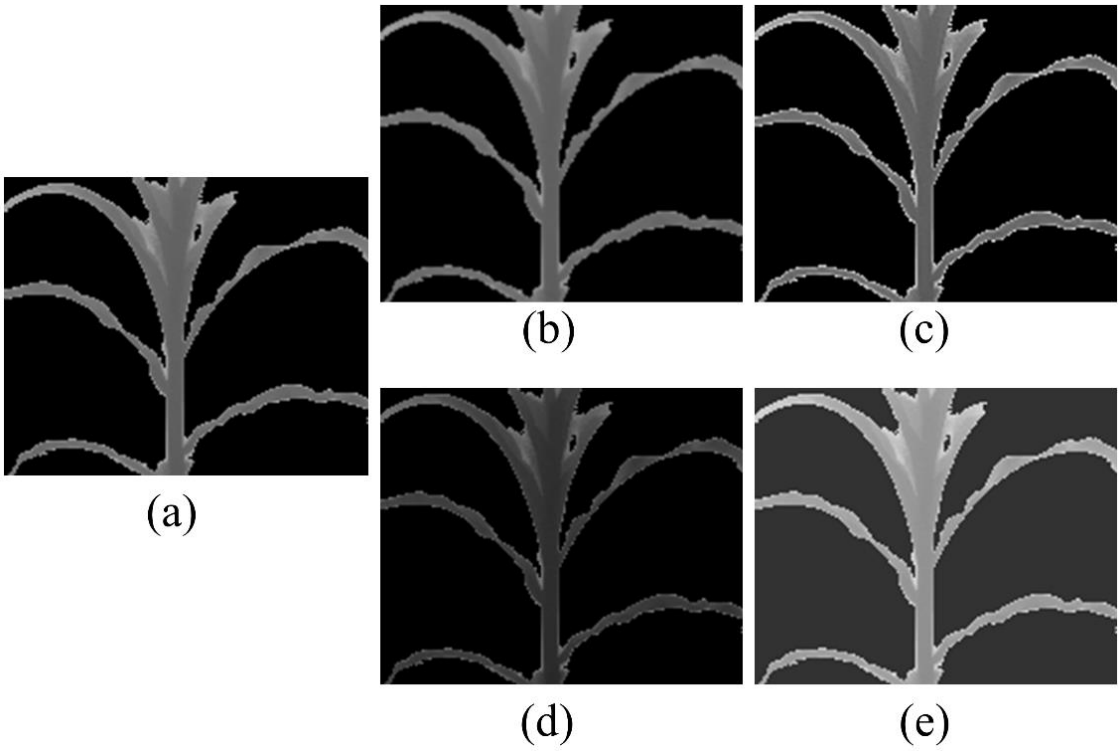

Fig. 3.7. The images before and after using augmentation technique (a) raw image (b) Blurred image (c) Sharpened image (d) Darkened image (e) Brightened image

Faster R-CNN technique was used for stem detection in the images. In this method, the image was provided as an input to a convolutional network which provided a convolutional feature map. Then a separate network was used to predict the region proposals. The predicted region proposals are then reshaped using a Region of Interest

(RoI) pooling layer which is then used to classify the image within the proposed region and predict the offset values for the bounding boxes. In this research, the network consisted of two convolutional layers, Region Proposal Network (RPN), RoI max pooling, and two fully-connected layers. The convolutional layers had 32 filters with size of 3×3, padding of 1, and ReLu (Rectifier Linear Unit) activation function. The output of the convolutional layers was fed to RPN, and then RoI max pooling with the size of 3 and stride of 2. The first fully connected-layer had 64 neurons with ReLu, and the second (last) layer had 2 classes (background and stem) with Softmax as loss layer (cross-entropy). Stochastic Gradient Descent with Momentum (SGDM) of 0.9, 100 epochs, batch size of 32, and initial learning rate of 0.001 was used as the optimizer for the network. The network was trained using 240 training images and its output was a detector which could detect the stem in the image (bounding box) and also to predict the class object (background or stem). Fig. 3.8 illustrates the architecture of the network. The average loss, and accuracy for training set were 0.434, and 97.6 % respectively. The detector was used to find a bounding box as stem region in a testing image. Several bounding boxes were found as stems by the detector. The bounding box which had the highest score was determined as the stem (Fig. 3.9). Sixty testing images were used to evaluate the performance of the network. The results showed that the accuracy and average precision of the network were 93%, and 0.81. A laptop with Intel Core i7 Processor (2.5 GHz) and 8 GB RAM was used to accomplish the training process of the network.

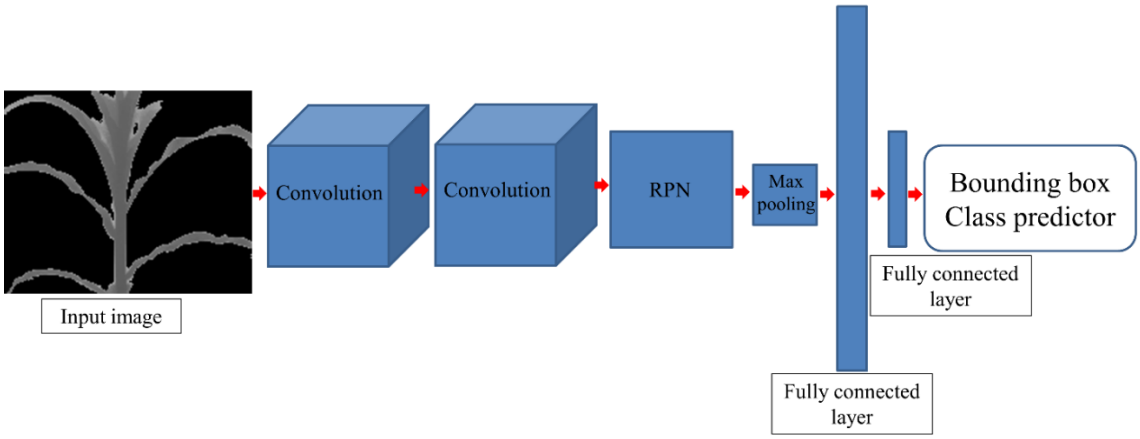

Fig. 3.8. The architecture of Faster R-CNN

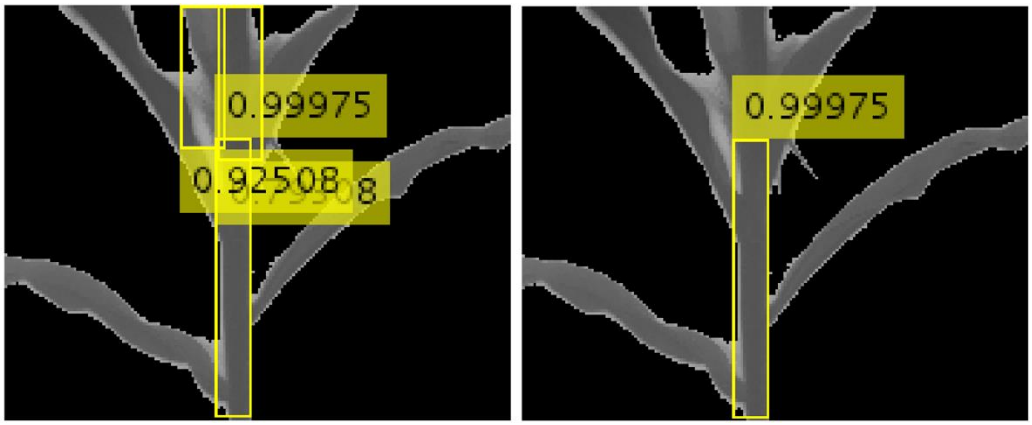

Fig. 3.9. Several bounding boxes were found after applying the detector (left), and stem was detected with the bounding box having the highest score (right)

Determine the grasping point on stem: Image processing toolbox in MATLAB (version 2018, MathWorks) was used to segment the plant from the background in the image and to determine the grasping point on the stem. A gray-scale image was created using a threshold for Z channel (the distance of the plant to the camera in Z direction) of the scene (Fig. 3.10a). Then the gray-scale image was converted to binary image (Fig. 3.10b). Deep learning technique (Faster R-CNN) was applied to detect the stem in the

image. The vertical lines of the bounding box were determined as stem's vertical edges (Fig. 3.10c).

The stem was removed from the binary image (after finding the vertical edges of the stem) and the most bottom leaf was labeled as the first leaf. The most bottom pixel of the first leaf which is connected to the stem was found. A horizontal line was drawn from the pixel which is used to find the proper grasping region of stem. The robotic system can grasp the stem from its grasping region without hitting the leaves (Fig. 3.10c). Thus, to detect the stem grasping area, all pixels in the binary image of the plant were removed except the pixels which was located between the stem's vertical edges and under the horizontal line (Fig. 3.10e). The coordinates of the center point of the stem grasping area in the image was determined as the grasping point (Fig. 3.10f). Then the XYZ coordinates (3D coordinates) of the grasping point relative to the center of the camera's coordinate system were found using XYZ channels of the scene, which was provided by the TOF camera.

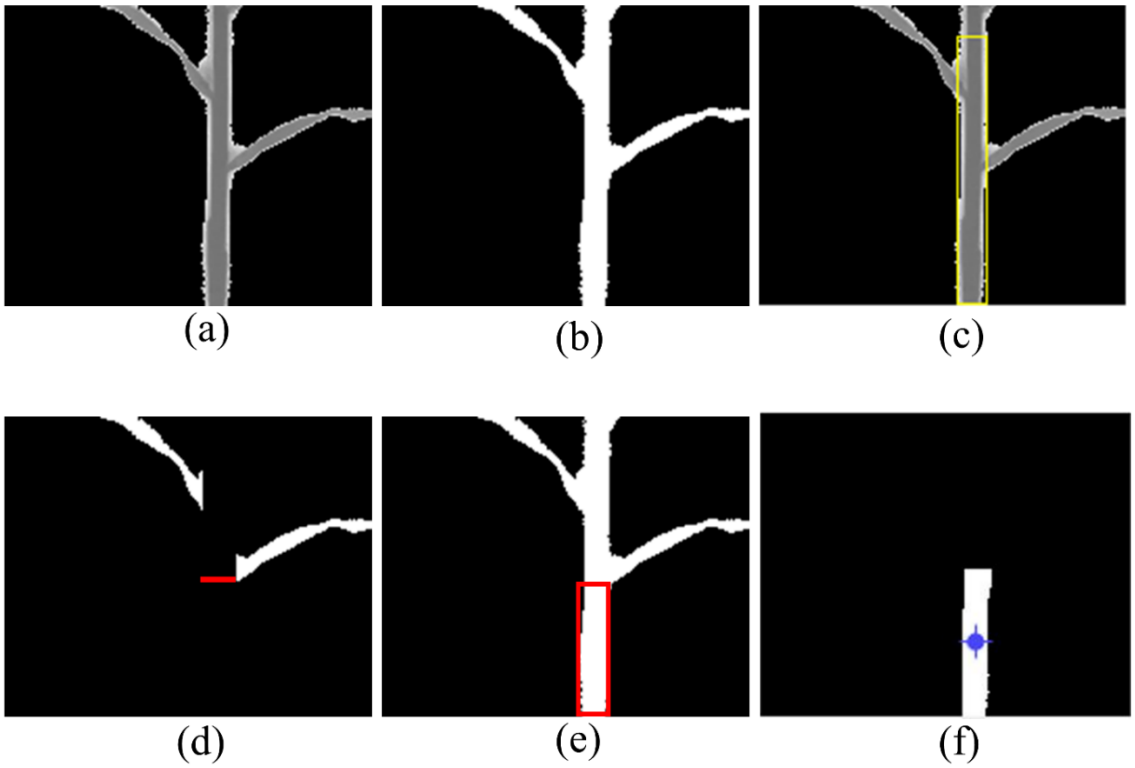

Fig. 3.10. Find the grasping point on the stem (a) Plant segmentation from the background (gray-scale image) (b) Binary image of the plant (c) Deep learning stem detection (determine stem vertical edges) (d) Find the horizontal line which is used to find stem grasping area (e) Stem grasping area (f) Stem grasping point

Inverse kinematics of the robotic manipulator: A transformation matrix was created based on the translation and rotation of the camera's coordinate system and robotic manipulator's coordinate system to find the 3D coordinates of the grasping point relative to the robotics manipulator's coordinate system (Eq. 3.3).

$$^{R}P = {}^{R}_{C}T \times {}^{C}P \tag{3.3}$$

Where:

$$ {}^{R}_{C}T = \begin{bmatrix} 1 & 0 & 0 & P_x \\ 0 & \cos(90) & -\sin(90) & P_y \\ 0 & \sin(90) & \cos(90) & P_z \\ 0 & 0 & 0 & 1 \end{bmatrix} $$

${}^{R}P$, ${}^{R}_{C}T$, and ${}^{C}P$ are the 3D coordinate of the grasping point relative to the center of robotic manipulator's system, the transformation matrix, and the 3D coordinates of the grasping point relative to the center of camera's coordinate system. P_x, P_y, and P_z are the distance between the coordinate system of the camera and robotic manipulator in X, Y, and Z directions.

The geometric approach in inverse kinematics was used to calculate the angle of the first three joints of the robotic manipulator for grasping process of the stem. The angle of the forth joint was a constant value such that the end-effector of the robotic manipulator was parallel relative to horizontal plane at the beginning and the forth joint angle was not changed during grasping process (Fig. 3.11).

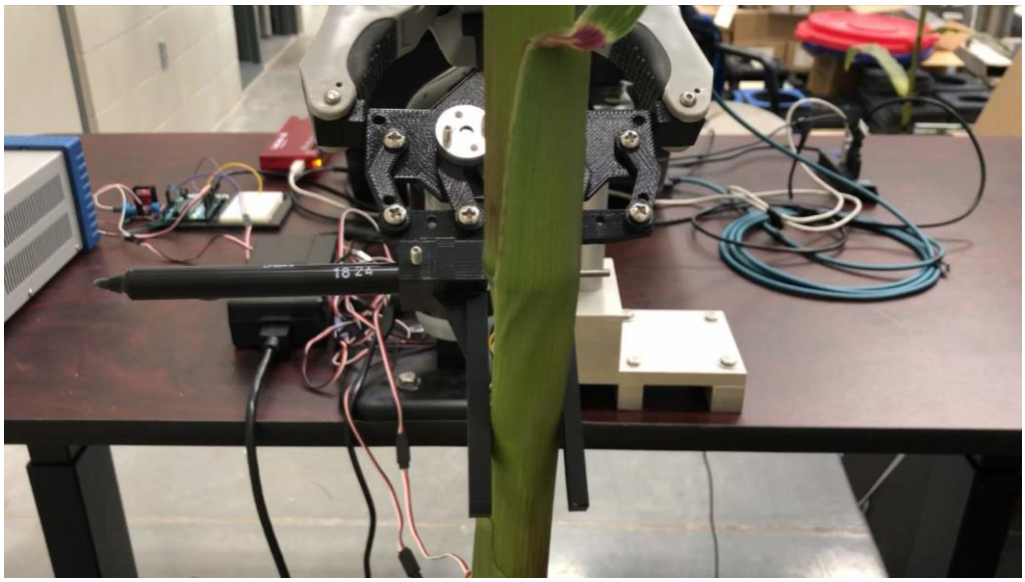

Fig. 3.11. The robotic manipulator grasped the stem to take its diameter measurement

Control the movement of the gripper's claws: An Arduino program was developed to control (open and close) the claws of the gripper. The output of the DC motor's encoder which shows the position of the motor was used to stop the linear movement of the claws at the end of the opening process when the claws are fully opened, and also at the end of the closing (grasping) process to avoid pressing and damage the stem. For this purpose, the program compares two consecutive readings of the encoder. If the readings are equal, then it can be identified that the motor is stalling as the resistance force exerted when the grippers are in contact with the stem or it is fully opened, as such it will be stopped. To open and close the claws using MATLAB, serial communication was used for MATLAB-Arduino communication. MATLAB Support Package for Arduino was used to communicate between MATLAB and Arduino.

3.2.3 GREENHOUSE EXPERIMENT AND DATA COLLECTION

A validation experiment was conducted in the Greenhouse Innovation Center of the University of Nebraska-Lincoln to assess the robotic system. For this purpose, two different lines of maize (B73 and Oh47) and two different lines of sorghum (Simon and Grassl) were selected (Fig. 3.12). Eight plants for each line of maize and sorghum were grown and 32 plants in total were used for the experiment.

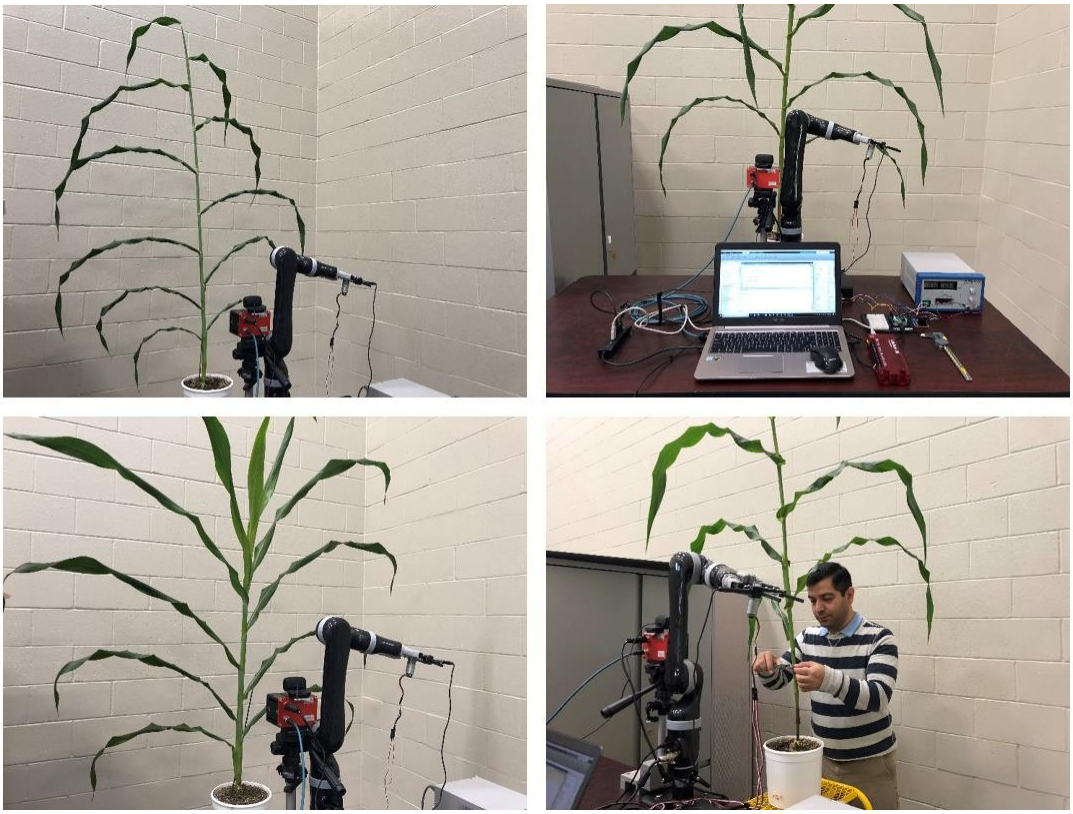

Fig. 3.12. Two different lines of sorghum (first column) and two different lines of maize (right column) which were used in the experiment

The experiment was done in six weeks (three weeks for maize and three weeks for sorghum) to create more variability for stem diameter measurement. One day per week was chosen to measure the stem diameter of sixteen plants. In total, the stem diameter of 96 samples were measured during the experiment. To take the automated measurements, two or three leaves of the plant from its down side were pruned to avoid hitting the pot by the robotic manipulator. For each plant, after taking the robotic measurement, the ground-truth (manual) measurement of stem diameter on the grasping point was taken by a digital caliper (Model: Brown & Sharpe 00590091, Hexagon Manufacturing Inc., TESA USA,

North Kingstown, RI, USA). The ground-truth measurement was used to evaluate the performance of the robotic system for measuring the stem diameter (Fig. 3.13).

Fig. 3.13. The manual measurement of stem diameter using a digital caliper

3.3 RESULTS AND DISCUSSION

Table 3.1 shows the time statistic for stem detection using deep learning, image processing to determine the grasping point on the stem, Inverse kinematics, stem grasping, sensing process, and total execution time.

Table 3.1. The time statistic for different steps of the automated stem measurement

Time (s)	Statistic	Maize	Sorghum	Overall
Stem detection (Deep learning)	Maximum	1.63	1.77	1.77
	Minimum	1.22	1.25	1.22
	Average	1.31	1.33	1.32
	Standard deviation	0.089	0.108	0.099
Determine grasping point on the stem (Image processing)	Maximum	3.09	3.18	3.18
	Minimum	2.51	2.62	2.51
	Average	2.74	2.77	2.76

	Standard deviation	0.105	0.109	0.108
Inverse kinematics	Maximum	0.004	0.004	0.004
	Minimum	0.002	0.002	0.002
	Average	0.003	0.003	0.003
	Standard deviation	0	0	0
Stem grasping	Maximum	45.1	45.2	45.2
	Minimum	41.7	40.9	40.9
	Average	42.5	42.5	42.5
	Standard deviation	0.785	0.950	0.867
Sensing process	Maximum	0.045	0.040	0.045
	Minimum	0.030	0.031	0.030
	Average	0.034	0.033	0.033
	Standard deviation	0.003	0.002	0.003
Total execution time	Maximum	47.6	48.0	48.0
	Minimum	44.4	43.7	43.7
	Average	45.3	45.3	45.3
	Standard deviation	0.797	0.946	0.871

It can be seen that the stem grasping, which the robotic manipulator was moved to grasp the stem and back to its first position after taking the measurement, has the longest time. The reason for that is the movement speed of the robotic manipulator for grasping process was reduced in order to avoid hitting and damage the plant by the robotic manipulator. The stem detection, determine grasping point on the stem, and sensing process took short times which illustrates the potential of the system for real-time stem detection and localization, and also stem diameter measurement.

The automated measurement takes more time (total execution time) compare to a manual measurement (less than 10 s). From the table above, it can be found that the long time for stem grasping step leads to long total execution time. The path planning technique can be used to find the optimal grasping path without hitting the plant to minimize the time for stem grasping process. Moreover, the time for stem detection using deep learning is short enough to have real-time measurements, however it can be reduced by using more training dataset with a deeper network or using transfer learning technique to train the network.

Faster R-CNN method successfully detect the stem (either vertical or tilted) for all plants. Furthermore, the robotic system could grasp the stem of all plants successfully.

Fig. 3.14 shows the correlation between the automated and manual measurement for maize, sorghum, and overall maize and sorghum plants.

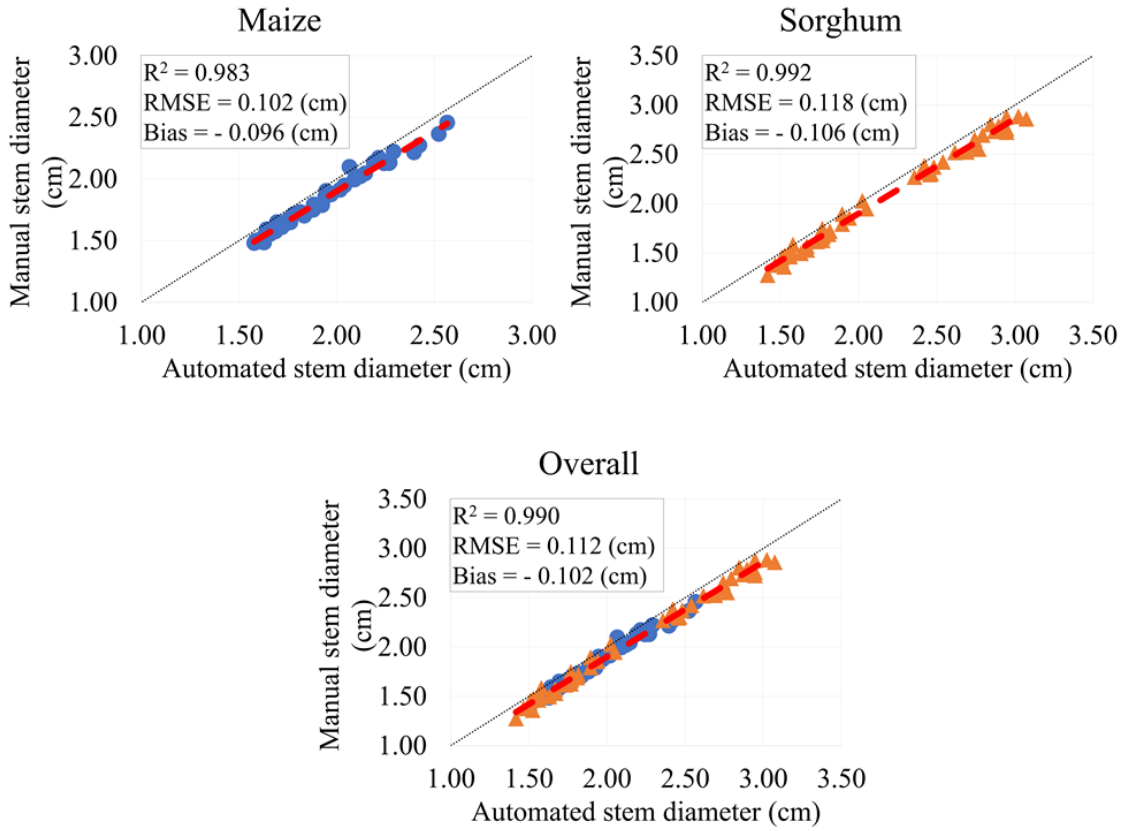

Fig. 3.14. The scatterplots of manual and automated measurements of stem diameter for maize (left), sorghum (right), and overall maize and sorghum (bottom)

It can be seen that the automated and manual measurements were highly linearly correlated (R^2=0.983 for maize, R^2=0.992 for sorghum, and R^2=0.990 for maize and sorghum together). Moreover, it can be found that RMSE (Root Mean Square Error) between two sets of measurements was very small value (0.102, 0.118, 0.112 cm for maize, sorghum, and maize and sorghum together). Furthermore, there was also a very small bias between the robotized and manual measurement (-0.096, -0.106, -0.102 cm for maize, sorghum, and overall maize and sorghum). It can be concluded that the robotic system could accurately measure the stem diameter for all plants during the experiment.

3.4 CONCLUSIONS

In this research, a plant phenotyping robotic system was developed to automatically measure stem diameter of plant. The robotic system consisted of a 4 DOF robotic manipulator, a TOF camera for vision system, a linear potentiometer (LP) sensor to measure the stem diameter, a custom designed gripper to integrate the LP sensor to the robotic manipulator, and an Arduino UNO to control the gripper. A deep learning algorithm (based on Faster R-CNN) was developed to detect the stem in the image and find the grasping point on the stem. An experiment was conducted in the greenhouse using maize and sorghum plants to compare the robotic and manual (ground-truth) measurements of stem diameter and evaluate the performance of the system. The results showed a very high linear correlation with very small bias and RMSE between the automated and manual measurements. The system could successfully detect and localize, and also grasp the stem for all plants during the experiment. The average times for stem detection (using deep learning technique), sensing process (measure stem diameter using LP sensor), and total execution time (grasp the stem and measure its diameter) for overall maize and sorghum plants were 1.32, 0.033, 45.3 s respectively. The times for stem detection and sensing process were very short which is important for real-time stem detection and localization, and also stem diameter measurement. Since the need of a laborer to measure stem diameter manually was removed using the robotic system which could automatically gathers data, the tediousness of collecting data was significantly reduced. This robotic system shows a potential to complement image-based high-throughput plant phenotyping by real-time measurement of stem diameter automatically and accurately.

CHAPTER 4

CONCLUSION

The goal of the discussed study was to develop a robotic system for *in vivo*, human-like phenotyping of maize and sorghum plants in the greenhouse which could collect phenotypic data less tediously compared to manual measurements. The goal was achieved by accomplishing two different objectives. The first objective was to develop an automated robotic system which was able to measure leaf attributes such as leaf VisNIR (visible and near infrared) and leaf temperature simultaneously; and the second objective was to develop a robotic system which could measure the stem diameter of plants automatically.

For the first objective, a 4 DOF robotic manipulator, a TOF camera for vision, a portable spectrometer with a bifurcated optical fiber cable for leaf reflectance measurement, a thermistor for leaf temperature measurement, and a customized gripper to integrate the sensors to the end effector of the robotic manipulator were used in the robotic system. An algorithm based on image processing technique was developed to find the 3D coordinates of the grasping point on leaves. The robotic system acquired leaf reflectance and leaf temperature simultaneously. The performance of the phenotyping robot was tested in the greenhouse using maize and sorghum plants. The comparison results for leaf temperature showed a significant correlation between the automated and ground-truth measurements. The PLSR method was used to predict several leaf properties such as chlorophyll, water content, nitrogen, phosphorus, and potassium concentrations from the leaf reflectance by the phenotyping robot. The chlorophyll, water content and

potassium were estimated with moderate success, whereas the nitrogen and phosphorus estimations were poor.

For the second objective, the phenotyping robot compromised of a 4 DOF robotic manipulator, a 3D TOF camera, a linear potentiometer (LP) sensor to measure the stem diameter, a custom designed gripper to integrate the LP sensor to the robotic manipulator, and an Arduino Uno to control the gripper. A deep learning algorithm (based on Faster R-CNN) was developed to detect the stem in the image and find the grasping point on the stem. An experiment was conducted in the greenhouse using maize and sorghum plants to compare the robotic and manual (ground-truth) measurements of stem diameter to evaluate the system performance. The experimental results demonstrated that the deep learning algorithm could detect the stem of all plants successfully. Moreover, a high correlation between the automated and manual measurements was achieved and it illustrated that the robotic system could measure the stem diameter accurately.

Since both robotic systems no longer needed a laborer for collecting data and phenotypes were automatically collected by the systems, the tediousness was significantly decreased compared to manual measurements.

The phenotyping robots showed a potential to complement the traditional image-based high-throughput plant phenotyping in greenhouses by measuring the physiological and biochemical traits of leaf and stem directly and automatically.

REFERENCES

Ahlin, K., Joffe, B., Hu, A.-P., McMurray, G., Sadegh, N., 2016. Autonomous Leaf Picking Using Deep Learning and Visual-Servoing. IFAC-PapersOnLine 49, 177–183. https://doi.org/https://doi.org/10.1016/j.ifacol.2016.10.033

Alenyà, G., Dellen, B., Torras, C., 2011. 3D modelling of leaves from color and ToF data for robotized plant measuring, in: 2011 IEEE International Conference on Robotics and Automation. pp. 3408–3414. https://doi.org/10.1109/ICRA.2011.5980092

Alenyà Ribas, G., Dellen, B., Foix Salmerón, S., Torras, C., 2012. Robotic leaf probing via segmentation of range data into surface patches, in: Proceedings of the 2012 IROS Workshop on Agricultural Robotics: Enabling Safe, Efficient, Affordable Robots for Food Production. pp. 1–6.

Andrade-Sanchez, P., Gore, M.A., Heun, J.T., Thorp, K.R., Carmo-Silva, A.E., French, A.N., Salvucci, M.E., White, J.W., 2013. Development and evaluation of a field-based high-throughput phenotyping platform. Funct. Plant Biol. 41, 68–79.

Apogee Instruments, 2019. Owner's Manual Temperature Sensors [Online]. Available: https://www.apogeeinstruments.com/content/ST-100-110-200-300-manual.pdf.

Bai, G., Ge, Y., Hussain, W., Baenziger, P.S., Graef, G., 2016. A multi-sensor system for high throughput field phenotyping in soybean and wheat breeding. Comput. Electron. Agric. 128, 181–192. https://doi.org/https://doi.org/10.1016/j.compag.2016.08.021

Bai, G., Ge, Y., Scoby, D., Leavitt, B., Stoerger, V., Kirchgessner, N., Irmak, S., Graef, G., Schnable, J., Awada, T., 2019. NU-Spidercam: A large-scale, cable-driven, integrated sensing and robotic system for advanced phenotyping, remote sensing, and agronomic research. Computers and Electronics in Agriculture 160, 71-81.

Bao, Y., Tang, L., Breitzman, M.W., Salas Fernandez, M.G., Schnable, P.S., 2019. Field-based robotic phenotyping of sorghum plant architecture using stereo vision. J. F. Robot. 36, 397–415.

Bao, Y., Tang, L., Shah, D., 2017. Robotic 3D Plant Perception and Leaf Probing with Collision-Free Motion Planning for Automated Indoor Plant Phenotyping. 2017 ASABE Annu. Int. Meet., ASABE Paper No. 1700369. https://doi.org/https://doi.org/10.13031/aim.201700369

Barker, J., Zhang, N., Sharon, J., Steeves, R., Wang, X., Wei, Y., Poland, J., 2016. Development of a field-based high-throughput mobile phenotyping platform. Comput. Electron. Agric. 122, 74–85. https://doi.org/https://doi.org/10.1016/j.compag.2016.01.017

Baweja, H.S., Parhar, T., Mirbod, O., Nuske, S., 2018. StalkNet: A Deep Learning Pipeline for High-Throughput Measurement of Plant Stalk Count and Stalk Width BT - Field and Service Robotics, in: Hutter, M., Siegwart, R. (Eds.), . Springer International Publishing, Cham, pp. 271–284.

Berni, J.A.J., Zarco-Tejada, P.J., Suarez, L., Fereres, E., 2009. Thermal and Narrowband Multispectral Remote Sensing for Vegetation Monitoring From an Unmanned Aerial Vehicle. IEEE Trans. Geosci. Remote Sens. 47, 722–738. https://doi.org/10.1109/TGRS.2008.2010457

Busemeyer, L., Mentrup, D., Möller, K., Wunder, E., Alheit, K., Hahn, V., Maurer, P.H., Reif, C.J., Würschum, T., Müller, J., Rahe, F., Ruckelshausen, A., 2013. BreedVision — A Multi-Sensor Platform for Non-Destructive Field-Based Phenotyping in Plant Breeding. Sensors. https://doi.org/10.3390/s130302830

Chaivivatrakul, S., Tang, L., Dailey, M.N., Nakarmi, A.D., 2014. Automatic morphological trait characterization for corn plants via 3D holographic reconstruction. Comput. Electron. Agric. 109, 109–123.

Chapman, C.S., Merz, T., Chan, A., Jackway, P., Hrabar, S., Dreccer, F.M., Holland, E., Zheng, B., Ling, J.T., Jimenez-Berni, J., 2014. Pheno-Copter: A Low-Altitude, Autonomous Remote-Sensing Robotic Helicopter for High-Throughput Field-Based Phenotyping. Agronomy. https://doi.org/10.3390/agronomy4020279

Chaudhury, A., Ward, C., Talasaz, A., Ivanov, A.G., Brophy, M., Grodzinski, B., Huner, N., Patel, R. V, Barron, J.L., 2017. Machine Vision System for 3D Plant Phenotyping. arXiv Prepr. arXiv1705.00540.

Chaves, M.M., Maroco, J.P., Pereira, J.S., 2003. Understanding plant responses to drought—from genes to the whole plant. Funct. plant Biol. 30, 239–264.

Choudhury, S. Das, Stoerger, V., Samal, A., Schnable, J.C., Liang, Z., Yu, J.-G., 2016. Automated vegetative stage phenotyping analysis of maize plants using visible light images, in: KDD Workshop on Data Science for Food, Energy and Water, San Francisco, California, USA.

Das Choudhury, S., Goswami, S., Bashyam, S., Samal, A., Awada, T., 2017. Automated Stem Angle Determination for Temporal Plant Phenotyping Analysis, in: Proceedings of the IEEE International Conference on Computer Vision. pp. 2022–2029.

Dengyu, X., Liang, G., Chengliang, L., Yixiang, H., 2016. Phenotype-based Robotic Screening Platform for Leafy Plant Breeding. IFAC-PapersOnLine 49, 237–241. https://doi.org/https://doi.org/10.1016/j.ifacol.2016.10.044

Dhondt, S., Wuyts, N., Inzé, D., 2013. Cell to whole-plant phenotyping: the best is yet to come. Trends Plant Sci. 18, 428–439. https://doi.org/https://doi.org/10.1016/j.tplants.2013.04.008

Fahlgren, N., Feldman, M., Gehan, M.A., Wilson, M.S., Shyu, C., Bryant, D.W., Hill, S.T., McEntee, C.J., Warnasooriya, S.N., Kumar, I., Ficor, T., Turnipseed, S., Gilbert, K.B., Brutnell, T.P., Carrington, J.C., Mockler, T.C., Baxter, I., 2015a. A Versatile Phenotyping System and Analytics Platform Reveals Diverse Temporal Responses to Water Availability in Setaria. Mol. Plant 8, 1520–1535. https://doi.org/https://doi.org/10.1016/j.molp.2015.06.005

Fahlgren, N., Gehan, M.A., Baxter, I., 2015b. Lights, camera, action: high-throughput plant phenotyping is ready for a close-up. Curr. Opin. Plant Biol. 24, 93–99. https://doi.org/https://doi.org/10.1016/j.pbi.2015.02.006

Fehr, W., 1991. Principles of cultivar development: theory and technique. Macmillian Publishing Company.

Fischer, G., 2009. World food and agriculture to 2030/50, in: Technical Paper from the Expert Meeting on How to Feed the World In. pp. 24–26.

Foix, S., Alenyà, G., Torras, C., 2018. Task-driven active sensing framework applied to leaf probing. Comput. Electron. Agric. https://doi.org/https://doi.org/10.1016/j.compag.2018.01.020

Foix, S., Alenyà, G., Torras, C., 2015. 3D Sensor planning framework for leaf probing, in: 2015 IEEE/RSJ International Conference on Intelligent Robots and Systems (IROS). pp. 6501–6506. https://doi.org/10.1109/IROS.2015.7354306

Fourcaud, T., Zhang, X., Stokes, A., Lambers, H., Körner, C., 2008. Plant Growth Modelling and Applications: The Increasing Importance of Plant Architecture in Growth Models. Ann. Bot. 101, 1053–1063.

Furbank, R.T., Tester, M., 2011. Phenomics – technologies to relieve the phenotyping bottleneck. Trends Plant Sci. 16, 635–644. https://doi.org/https://doi.org/10.1016/j.tplants.2011.09.005

Gage, J.L., Miller, N.D., Spalding, E.P., Kaeppler, S.M., de Leon, N., 2017. TIPS: a system for automated image-based phenotyping of maize tassels. Plant Methods 13, 21. https://doi.org/10.1186/s13007-017-0172-8

Ghosal, S., Blystone, D., Singh, A.K., Ganapathysubramanian, B., Singh, A., Sarkar, S., 2018. An explainable deep machine vision framework for plant stress phenotyping. Proc. Natl. Acad. Sci. 115, 4613 LP-4618. https://doi.org/10.1073/pnas.1716999115

Granier, C., Tardieu, F., 2009. Multi-scale phenotyping of leaf expansion in response to environmental changes: the whole is more than the sum of parts. Plant. Cell Environ. 32, 1175–1184.

Hairmansis, A., Berger, B., Tester, M., Roy, S.J., 2014. Image-based phenotyping for non-destructive screening of different salinity tolerance traits in rice. Rice 7, 16. https://doi.org/10.1186/s12284-014-0016-3

Holman, H.F., Riche, B.A., Michalski, A., Castle, M., Wooster, J.M., Hawkesford, J.M., 2016. High Throughput Field Phenotyping of Wheat Plant Height and Growth Rate in Field Plot Trials Using UAV Based Remote Sensing. Remote Sens. https://doi.org/10.3390/rs8121031

Jannink, J.-L., Lorenz, A.J., Iwata, H., 2010. Genomic selection in plant breeding: from theory to practice. Brief. Funct. Genomics 9, 166–177. https://doi.org/10.1093/bfgp/elq001

Jin, S., Su, Y., Gao, S., Wu, F., Hu, T., Liu, J., Li, W., Wang, D., Chen, S., Jiang, Y.,

Pang, S., Guo, Q., 2018. Deep Learning: Individual Maize Segmentation From Terrestrial Lidar Data Using Faster R-CNN and Regional Growth Algorithms. Front. Plant Sci.

Jin, S., Su, Y., Wu, F., Pang, S., Gao, S., Hu, T., Liu, J., Guo, Q., 2019. Stem–Leaf Segmentation and Phenotypic Trait Extraction of Individual Maize Using Terrestrial LiDAR Data. IEEE Trans. Geosci. Remote Sens. 57, 1336–1346. https://doi.org/10.1109/TGRS.2018.2866056

KINOVA, 2018. KINOVA MICO Robotic Arm User Guide [Online]. Available: https://www.kinovarobotics.com/sites/default/files/ULWS-RA-MIC-UG-INT-EN%20201804-1.0%20%28KINOVA%20MICO%E2%84%A2%20Robotic%20arm%20user%20guide%29_0.pdf.

Kuhn, M., Wing, J., Weston, S., Williams, A., Keefer, C., Engelhardt, A., Cooper, T., Mayer, Z., Kenkel, B., Team, the R.C., Benesty, M., Lescarbeau, R., Ziem, A., Scrucca, L., Tang, Y., Candan, C., Hunt., T., 2017. caret: Classification and Regression Training.

LabJack, 2016. U6 Datasheet [Online]. Avaialble: https://labjack.com/support/datasheets/u6.

Li, J., Shi, Y., Veeranampalayam-Sivakumar, A.-N., Schachtman, D.P., 2018. Elucidating Sorghum Biomass, Nitrogen and Chlorophyll Contents With Spectral and Morphological Traits Derived From Unmanned Aircraft System. Front. Plant Sci. 9, 1406. https://doi.org/10.3389/fpls.2018.01406

Li, L., Zhang, Q., Huang, D., 2014. A Review of Imaging Techniques for Plant Phenotyping. Sensors. https://doi.org/10.3390/s141120078

Lu, H., Tang, L., Whitham, A.S., Mei, Y., 2017. A Robotic Platform for Corn Seedling Morphological Traits Characterization. Sensors. https://doi.org/10.3390/s17092082

McMullen, M.D., Kresovich, S., Villeda, H.S., Bradbury, P., Li, H., Sun, Q., Flint-Garcia, S., Thornsberry, J., Acharya, C., Bottoms, C., Brown, P., Browne, C., Eller, M., Guill, K., Harjes, C., Kroon, D., Lepak, N., Mitchell, S.E., Peterson, B., Pressoir, G., Romero, S., Rosas, M.O., Salvo, S., Yates, H., Hanson, M., Jones, E., Smith, S., Glaubitz, J.C., Goodman, M., Ware, D., Holland, J.B., Buckler, E.S., 2009. Genetic Properties of the Maize Nested Association Mapping Population. Science (80-.). 325, 737 LP-740. https://doi.org/10.1126/science.1174320

MESA Imaging, 2016. SR4000/SR4500 User Manual V 3.0 [Online]. Available: http://www.realtechsupport.org/UB/SR/range_finding/SR4000_SR4500_Manual.pdf.

Mevik, B.-H., Wehrens, R., Liland, K.H., 2016. pls: Partial Least Squares and Principal Component Regression.

Montes, J.M., Melchinger, A.E., Reif, J.C., 2007. Novel throughput phenotyping platforms in plant genetic studies. Trends Plant Sci. 12, 433–436.

https://doi.org/https://doi.org/10.1016/j.tplants.2007.08.006

Mueller-Sim, T., Jenkins, M., Abel, J., Kantor, G., 2017. The Robotanist: A ground-based agricultural robot for high-throughput crop phenotyping, in: 2017 IEEE International Conference on Robotics and Automation (ICRA). pp. 3634–3639. https://doi.org/10.1109/ICRA.2017.7989418

OcenOptics, 2015. Flame Miniature Spectrometer User Manual [Online]. Available: https://oceanoptics.com/wp-content/uploads/FlameIO.pdf.

OMEGA Engineering, 2018. LP 803/LP 804 Instruction Sheet [Online]. Available: https://assets.omega.com/manuals/M4097.pdf.

Pandey, P., Ge, Y., Stoerger, V., Schnable, J.C., 2017. High Throughput In vivo Analysis of Plant Leaf Chemical Properties Using Hyperspectral Imaging. Front. Plant Sci.

Phillips, R.L., 2010. Mobilizing science to break yield barriers. Crop Sci. 50, S-99.

Poehlman, J.M., 2013. Breeding field crops. Springer Science & Business Media.

Pound, M.P., Atkinson, J.A., Townsend, A.J., Wilson, M.H., Griffiths, M., Jackson, A.S., Bulat, A., Tzimiropoulos, G., Wells, D.M., Murchie, E.H., Pridmore, T.P., French, A.P., 2017. Deep machine learning provides state-of-the-art performance in image-based plant phenotyping. Gigascience 6, gix083-gix083.

Rahaman, M.M., Chen, D., Gillani, Z., Klukas, C., Chen, M., 2015. Advanced phenotyping and phenotype data analysis for the study of plant growth and development. Front. Plant Sci.

Richards, R.A., Rebetzke, G.J., Watt, M., Condon, A.G. (Tony), Spielmeyer, W., Dolferus, R., 2010. Breeding for improved water productivity in temperate cereals: phenotyping, quantitative trait loci, markers and the selection environment. Funct. Plant Biol. 37, 85–97.

Schepers, J.S., Holland, K.H., Francis, D.D., 2017. Automated Measurement of Maize Stalk Diameter and Plant Spacing. Adv. Anim. Biosci. 8, 220–223. https://doi.org/DOI: 10.1017/S2040470017001170

Shafiekhani, A., Kadam, S., Fritschi, B.F., DeSouza, N.G., 2017. Vinobot and Vinoculer: Two Robotic Platforms for High-Throughput Field Phenotyping. Sensors. https://doi.org/10.3390/s17010214

Shah, D., Tang, L., Gai, J., Putta-Venkata, R., 2016. Development of a Mobile Robotic Phenotyping System for Growth Chamber-based Studies of Genotype x Environment Interactions. IFAC-PapersOnLine 49, 248–253. https://doi.org/https://doi.org/10.1016/j.ifacol.2016.10.046

Shakoor, N., Lee, S., Mockler, T.C., 2017. High throughput phenotyping to accelerate crop breeding and monitoring of diseases in the field. Curr. Opin. Plant Biol. 38, 184–192. https://doi.org/https://doi.org/10.1016/j.pbi.2017.05.006

Shi, Y., 2014. Corn Plant Location, Spacing and Stalk Diameter Measurement Using

Optical Sensing Technologies.

Thapa, S., Zhu, F., Walia, H., Yu, H., Ge, Y., 2018. A Novel LiDAR-Based Instrument for High-Throughput, 3D Measurement of Morphological Traits in Maize and Sorghum. Sensors (Basel). 18, 1187. https://doi.org/10.3390/s18041187

THORLABS, 2014. RP25 - Reflection Probe with Linear Leg [Online]. Available: https://www.thorlabs.com/thorproduct.cfm?partnumber=RP25.

THORLABS, 2016. SLS201 - Stabilized Light Source [Online]. Available: https://www.thorlabs.com/thorproduct.cfm?partnumber=SLS201.

Tsaftaris, S.A., Minervini, M., Scharr, H., 2016. Machine learning for plant phenotyping needs image processing. Trends Plant Sci. 21, 989–991.

Ubbens, J.R., Stavness, I., 2017. Deep Plant Phenomics: A Deep Learning Platform for Complex Plant Phenotyping Tasks. Front. Plant Sci.

Van Henten, E.J., Van Tuijl, B.A.J., Hoogakker, G.-J., Van Der Weerd, M.J., Hemming, J., Kornet, J.G., Bontsema, J., 2006. An Autonomous Robot for De-leafing Cucumber Plants grown in a High-wire Cultivation System. Biosyst. Eng. 94, 317–323. https://doi.org/https://doi.org/10.1016/j.biosystemseng.2006.03.005

Vázquez-Arellano, M., Paraforos, D.S., Reiser, D., Garrido-Izard, M., Griepentrog, H.W., 2018. Determination of stem position and height of reconstructed maize plants using a time-of-flight camera. Comput. Electron. Agric. 154, 276–288.

Vijayarangan, S., Sodhi, P., Kini, P., Bourne, J., Du, S., Sun, H., Poczos, B., Apostolopoulos, D., Wettergreen, D., 2018. High-Throughput Robotic Phenotyping of Energy Sorghum Crops BT - Field and Service Robotics, in: Hutter, M., Siegwart, R. (Eds.), . Springer International Publishing, Cham, pp. 99–113.

Virlet, N., Sabermanesh, K., Sadeghi-Tehran, P., Hawkesford, M.J., 2017. Field Scanalyzer: An automated robotic field phenotyping platform for detailed crop monitoring. Funct. Plant Biol. 44, 143–153.

Walter, A., Liebisch, F., Hund, A., 2015. Plant phenotyping: from bean weighing to image analysis. Plant Methods 11, 14. https://doi.org/10.1186/s13007-015-0056-8

White, J.W., Andrade-Sanchez, P., Gore, M.A., Bronson, K.F., Coffelt, T.A., Conley, M.M., Feldmann, K.A., French, A.N., Heun, J.T., Hunsaker, D.J., Jenks, M.A., Kimball, B.A., Roth, R.L., Strand, R.J., Thorp, K.R., Wall, G.W., Wang, G., 2012. Field-based phenomics for plant genetics research. F. Crop. Res. 133, 101–112. https://doi.org/https://doi.org/10.1016/j.fcr.2012.04.003

Yuan, W., Li, J., Bhatta, M., Shi, Y., Baenziger, S.P., Ge, Y., 2018. Wheat Height Estimation Using LiDAR in Comparison to Ultrasonic Sensor and UAS. Sensors. https://doi.org/10.3390/s18113731

Yue, J., Yang, G., Li, C., Li, Z., Wang, Y., Feng, H., Xu, B., 2017. Estimation of Winter Wheat Above-Ground Biomass Using Unmanned Aerial Vehicle-Based Snapshot Hyperspectral Sensor and Crop Height Improved Models. Remote Sens.

https://doi.org/10.3390/rs9070708

Zaman-Allah, M., Vergara, O., Araus, J.L., Tarekegne, A., Magorokosho, C., Zarco-Tejada, P.J., Hornero, A., Albà, A.H., Das, B., Craufurd, P., Olsen, M., Prasanna, B.M., Cairns, J., 2015. Unmanned aerial platform-based multi-spectral imaging for field phenotyping of maize. Plant Methods 11, 35. https://doi.org/10.1186/s13007-015-0078-2

Zeileis, A., Grothendieck, G., 2005. zoo: S3 Infrastructure for Regular and Irregular Time Series. J. Stat. Softw. 14, 1–27. https://doi.org/10.18637/jss.v014.i06

Zhang, X., Qiao, Y., Meng, F., Fan, C., Zhang, M., 2018. Identification of Maize Leaf Diseases Using Improved Deep Convolutional Neural Networks. IEEE Access 6, 30370–30377. https://doi.org/10.1109/ACCESS.2018.2844405